universität wien

MASTERARBEIT / MASTER'S THESIS

Titel der Masterarbeit / Title of the Master's Thesis

„Dissection of the SARS-CoV-2-specific and NK cell-mediated ADCC response"

verfasst von / submitted by

Danklmaier Vera, BSc

angestrebter akademischer Grad / in partial fulfilment of the requirements for the degree of

Master of Science (MSc)

Wien, 2022 / Vienna, 2022

Studienkennzahl lt. Studienblatt / degree programme code as it appears on the student record sheet:	UA 066 830
Studienrichtung lt. Studienblatt / degree programme as it appears on the student record sheet:	Masterstudium Molecular Microbiology, Microbial Ecology and Immunobiology
Betreut von / Supervisor:	Univ.-Prof. Dr. Elisabeth Puchhammer-Stöckl

Acknowledgements

First, I would like to thank Elisabeth Puchhammer-Stöckl for giving me the opportunity to do my master thesis at the Center for Virology and for the support.

Special thanks go to Hannes Vietzen for the supervision, guidance and great support throughout the whole project.

I also want to thank Ursula Sinzinger and Thomas Urbanek and all colleagues of the Center for Virology for the assistance and advices in the lab.

Further thanks go to my beloved fellow students, especially Simone, Helene, Cara and Thomas, for the great working atmosphere and for all the fun times inside and outside the lab.

My deepest thanks go to my family, my parents Andrea and Johann and my siblings Simon and Sarah and my friends for their love, support and encouragement during my studies.

List of Abbreviations

ACE2	Angiotensin-converting enzyme 2
ADCC	Antibody-dependent cellular cytotoxicity
ARDS	Acute respiratory distress syndrome
BALF	Bronchoalveolar lavage fluid
COVID-19	Coronavirus disease 2019
CTD	C-terminal domain
DC	Dendritic cell
DNA	Deoxyribonucleic acid
E-protein	Envelope protein
ELISA	Enzyme-linked immunosorbent assay
ELISpot	Enzyme-linked immune spot assay
EMA	European Medicines Agency
Fab domain	Fragment antigen-binding domain
Fc domain	Fragment crystallisable domain
FcγR	Fcγ receptor
FcγRIIIa	Fcγ receptor IIIa (CD16A)
GM-CSF	Granulocyte/macrophage colony-stimulating factor
HCoV	Human Coronaviruses
HR	Heptad repeats
ICU	Intensive care unit
IFN-β	Interferon beta
IFN-γ	Interferon gamma
Ig	Immunoglobulin
IgA	Immunoglobulin A
IgG	Immunoglobulin G
IgM	Immunoglobulin M
IL	Interleukin
M-protein	Membrane protein
MERS-CoV	Middle Eastern respiratory syndrome coronavirus
MFI	Mean fluorescence intensity

N-protein	Nucleocapsid protein
NK cells	Natural killer cells
ns	Not significant
nsp	Non-structural protein
NTD	N-terminal domain
ORF	Open reading frame
PBMC	Peripheral blood mononuclear cell
PCR	Polymerase chain reaction
RBD	Receptor-binding domain
RdRp	RNA-dependent RNA polymerase
RNA	Ribonucleic acid
RT-PCR	Reverse transcription polymerase chain reaction
S-protein	Spike protein
SARS-CoV-1	Severe acute respiratory syndrome coronavirus 1
SARS-CoV-2	Severe acute respiratory syndrome coronavirus 2
SNP	Single nucleotide polymorphism
TNF-α	Tumor-necrosis factor alpha
UTR	Untranslated region
VOC	Variant of concern
WHO	World Health Organization

Table of Contents

Abstract

The role of Natural Killer (NK) cells in the antibody-dependent cellular cytotoxicity (ADCC) in severe acute respiratory syndrome coronavirus 2 (SARS-CoV-2) infections is overall controversial. In the SARS-CoV-2-specific ADCC response, immunoglobulin G (IgG) antibodies bind to SARS-CoV-2-derived antigens and interact with the NK cell Fcγ receptor IIIa (FcγRIIIa), resulting in NK cell activation. Importantly, the FcγRIIIa shows a single nucleotide polymorphism (SNP) at amino acid position 158 resulting in a higher (FcγRIIIa-158-V/V) or lower (FcγRIIIa-158-F/F) extent of the ADCC response, which may affect the coronavirus disease 2019 (COVID-19) outcome. Thus, we aimed to assess the role of SARS-CoV-2-specific ADCC responses by analysing the NK cell activation depending on the FcγRIIIa-158 SNP and SARS-CoV-2-specific IgGs in hospitalized and non-hospitalized COVID-19 patients.

The distribution of the FcγRIIIa-158 variants was determined by Sanger-sequencing in both non-hospitalized and hospitalized COVID-19 patients. We investigated the extent of SARS-CoV-2-specific NK cell activation in the IgG-dependent ADCC response using cell activation assays, flow cytometry and ELISpot assays. Additionally, SARS-CoV-2-specific IgM, IgG and IgA seroconversion rates were determined by Enzyme-linked Immunosorbent Assay (ELISA).

In our study, we found that the FcγRIIIa-158-V/V variant was significantly overrepresented in hospitalized and deceased COVID-19 patients. Confirmed by a cell-based assay, the FcγRIIIa-158-V/V lead to higher NK cell activation. We detected an overall higher extent of NK cell activation in ADCC elicited by patients' plasma IgG antibodies in hospitalized COVID-19 patients. Based on our findings we conclude that severely diseased COVID-19 patients are hallmarked by a more potent SARS-CoV-2-specific, IgG-dependent ADCC response, which may result in severe COVID-19 manifestations.

Zusammenfassung

Die Rolle von Natürlichen Killerzellen (NK-Zellen) und deren Effektorfunktionen wie die antikörperabhängige zellvermittelte Zytotoxizität (ADCC) in ‚Severe Acute Respiratory Syndrome' Coronavirus 2 (SARS-CoV-2) Infektionen ist ambivalent. Bei der ADCC-Antwort binden SARS-CoV-2-spezifische Immunoglobulin G (IgG)-Antikörper an SARS-CoV-2-Antigene und interagieren mit dem NK-Zellrezeptor Fcγ Rezeptor IIIa (FcγRIIIa), was zur Aktivierung von NK-Zellen führt. Der FcγRIIIa Rezeptor zeigt einen Einzelnukleotid-Polymorphismus (SNP), der zu einer höheren oder niedrigeren SARS-CoV-2-spezifischen NK-Zellaktivierung in ADCC führt und dadurch möglicherweise den Verlauf der Coronavirus-Krankheit-2019 (COVID-19) beeinflusst. Das Ziel unserer Studie war es daher, die Rolle der SARS-CoV-2-spezifischen ADCC-Antwort zu analysieren, indem wir die NK-Zellaktivierung abhängig von SARS-CoV-2-spezifischen IgG-Antikörpern und vom FcγRIIIa SNP bei nicht-hospitalisierten und hospitalisierten COVID-19 PatientInnen bestimmten.

Die Verteilung der FcγRIIIa Varianten wurde zunächst mittels Sanger-Sequenzierung in nicht-hospitalisierten und hospitalisierten COVID-19 PatientInnen bestimmt. Das Gesamtausmaß der NK-Zellaktivierung in der IgG-abhängigen, SARS-CoV-2-spezifischen ADCC-Antwort von nicht-hospitalisierten und hospitalisierten COVID-19 PatientInnen wurde mittels Zellaktivierungsassay, Durchflusszytometrie und ELISpot gemessen. Außerdem wurden SARS-CoV-2-spezifische IgM, IgG und IgA Serokonversionsraten mittels Enzymgekoppeltem Immunadsorptionstest (ELISA) bestimmt.

Unsere Studie hat gezeigt, dass die Rezeptorvariante FcγRIIIa-158-V/V signifikant erhöht in den verstorbenen PatientInnen sowie PatientInnen mit schwerem COVID-19 Verlauf und Hospitalisierung vorkommt. Im Zell-basierten Assay konnten wir bestätigen, dass die FcγRIIIa-158-V/V Variante zu einer höheren NK-Zellaktivierung führte. In hospitalisierten COVID-19 PatientInnen wurde eine allgemein höhere SARS-CoV-2-spezifische, IgG- und NK-Zell-abhängige ADCC-Antwort gemessen. Basierend auf diesen Erkenntnissen kommen wir zum Schluss, dass eine stärkere SARS-CoV-2-spezifische ADCC-Antwort mit der Hospitalisierung von COVID-19-PatientInnen assoziiert ist, und zu schweren COVID-19 Manifestationen führen könnte.

1. Introduction

1.1 SARS-CoV-2

Severe acute respiratory syndrome Coronavirus 2 (SARS-CoV-2) is the causative agent of the coronavirus disease 2019 (COVID-19), which was declared as a pandemic by the World Health Organization (WHO) on March 11th, 2020 [1–3]. To the present day (14.12.2021), there have been over 270 Million cases worldwide confirmed, including over 5.3 Million COVID-19 associated deaths with both numbers still rising [4]. The emerging virus was first detected in patients with pneumonia in Wuhan in the Hubei province of China in December 2019. SARS-CoV-2 was identified and firstly described to be a novel, genetically distinct virus using next-generation sequencing (NGS) of bronchoalveolar lavage fluid (BALF) in nine patients [5]. SARS-CoV-2 is an airborne virus and is mainly transmitted through aerosols or respiratory droplets from coughing or sneezing and, to a lesser extent by direct human-to-human contact. SARS-CoV-2 enters the human host through the upper respiratory system, followed by a productive SARS-CoV-2 replication in both the upper and lower respiratory tract [2, 5].

1.1.1 SARS-CoV-2 phylogeny

Genetic analysis revealed the classification of SARS-CoV-2 in the order *Nidovirales*, the family *Coronaviridae*, the subfamily *Orthocoronavirinae*, the genus *Betacoronavirus* and the subgenus *Sarbecovirus*, as depicted in figure 1 [7, 8].

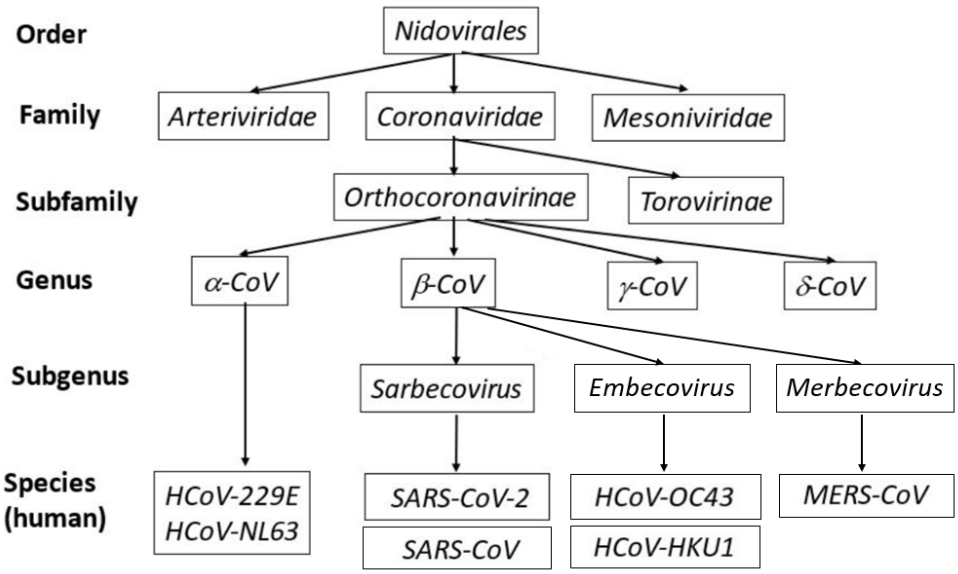

Figure 1: Phylogeny of human pathogenic Coronaviruses with the three major outbreak-causing *Betacoronavirus* species SARS-CoV-1 (Subgenus *Sarbecovirus*), MERS-CoV (Subgenus *Merbecovirus*) and SARS-CoV-2 (Subgenus *Sarbecovirus*) [Figure modified from Malik et al. [8]].

The suspected key reservoir of SARS-CoV-2 is the bat *Rhinolophus affinis* [9]. The bat coronavirus RaTG13 shares overall 91% sequence identity with the human SARS-CoV-2 and thus may represent the most likely origin of the SARS-CoV-2 outbreak [7]. SARS-CoV-2 is the third *Betacoronavirus* after severe acute respiratory syndrome Coronavirus (SARS-CoV-1) and Middle Eastern respiratory syndrome Coronavirus (MERS-CoV) that has caused a large-scale outbreak in the last 20 years. The reservoir hosts for both SARS-CoV-1 and MERS-CoV are assumed to be different bat families, such as *Rhinolophidae* for SARS-CoV-1 [10], with possible transmission of SARS-CoV-1 to humans via palm civets or a market with wild animals, such as raccoon dogs or ferret badgers [11] and of MERS-CoV via dromedary camels [12]. The SARS-CoV-1 outbreak originated in China in November 2002 and was declared to be over in July 2003 after 8096 reported cases, including 774 deaths (10% mortality) [12]. 10 years after the first emergence of SARS-CoV-1, in June 2012, MERS-CoV emerged in Saudi Arabia, which caused 2519 cases until January 2020, including 866 deaths, resulting in 34.4% mortality [13]. SARS-CoV-1 and MERS-CoV cause similar symptoms, such as coughing, fever, chills, malaise, myalgia and pneumonia. Compared to SARS-CoV-2, viral shedding in the upper respiratory tract is less efficient in SARS-CoV-1 and MERS-CoV infections, which explains why in contrast to SARS-CoV-1 and MERS-CoV, the emergence of SARS-CoV-2 resulted in a global pandemic [12].

Amongst less pathogenic human Coronavirus species, which seasonally cause mild respiratory symptoms are the human coronaviruses (HCoV) 229E and HCoV-NL63 of the *Alphacoronavirus* genus and HCoV-OC43 and HCoV-HKU1 of the *Betacoronavirus* genus [8].

1.1.2 SARS-CoV-2 genome and structural proteins

SARS-CoV-2 is characterized by an envelope that consists of the structural spike (S-), envelope (E-) and the membrane (M-) proteins (Figure 2a). The virus particle contains a positive sense single-stranded ribonucleic acid (RNA) with a length of 29.9 kilo bases that is encased by the nucleocapsid (N-) protein (Figure 2b) [2, 5, 14]. The S-protein, essential for viral entry into the host cell, is located in the open reading frame (ORF) 2. The E-protein, which is important for viral assembly and budding, is located in the ORF4. The M-protein, which plays also an important role for viral assembly, is encoded by the ORF5. The N-protein, which stabilizes the viral RNA, is located in the ORF9 [16]. The four structural proteins and accessory proteins are located at the 3' end, while sixteen non-structural proteins (nsp1-16), encoded in ORF1a (nsp1-11) and ORF1b (nsp12-16), are located at the 5' end of the SARS-CoV-2 genome. Nsp12, for instance, encodes the viral RNA-dependent RNA polymerase (RdRp) that is crucial for viral replication and transcription [16]. Both the 3'untranslated region (UTR) and the 5'UTR encode RNA elements that are relevant for transcription and replication of the SARS-CoV-2 genome [18, 19].

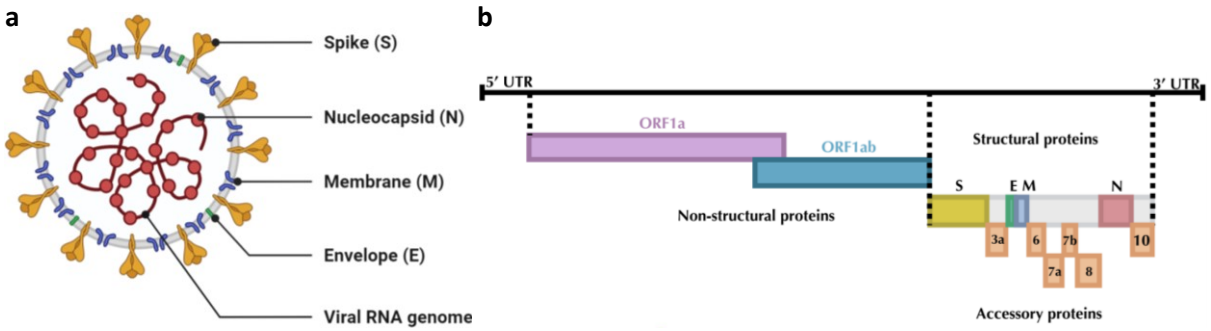

Figure 2: SARS-CoV-2 viral particle and genome. (a) Basic structure of the SARS-CoV-2 particle with the positive single-stranded RNA genome and the four structural proteins S, N, M and E [Figure adapted from "Human Coronavirus Structure" by Biorender.com (2021). Retrieved from https://app.biorender.com/biorender-templates [19]]. (b) SARS-CoV-2 genome architecture with the non-structural proteins in ORF1a and ORF1b at the 5'UTR and the structural proteins S, E, M and N and accessory proteins at the 3'UTR [Figure modified from Amor et al. [16]].

The S-protein of SARS-CoV-2 binds to the human angiotensin-converting enzyme 2 (ACE2) receptor, enabling fusion and viral cell entry. More detailed, the S-protein is a heterodimeric

glycoprotein with the two subunits S1 and S2 [20]. The S1 subunit is located distally, enabling the binding to the ACE2 receptor on the target cell. The two main structural domains of S1 are the C-terminal domain (S-CTD), also termed receptor-binding domain (RBD) [21], and the N-terminal galectin-like domain (S-NTD). The RBD determines the host virus range by the specific binding to target receptors, such as the ACE2 receptor, encoded by a broad range of mammalian species [20]. For example, the ACE2 of cats, dogs, minks, tigers, ferrets, macaques and grivets, resembles the human ACE2 at critical S-protein binding sites and these mammals are thus at risk for SARS-CoV-2 infections [22].

A first *in vitro* study by Wang and colleagues revealed that the S1 subunit and the RBD have a strong affinity to the human ACE2 [21]. The RBD contains the receptor-binding motif (RBM) that interacts with the N-terminal helix of ACE2. The specific role of S-NTD has not been assured yet. It may be essential to stabilize the S2 subunit in the pre-fusion state. It may also directly bind to the host receptor [20]. The S2 subunit is anchored in the viral membrane and mediates viral and cellular membrane fusion. The S2 subunit shows distinct pre-fusion and post-fusion conformations. The S2 subunit has four structural domains, which are a fusion peptide, two heptad repeats (HR1 and HR2) and a transmembrane region. Binding of the S1 subunit to the host receptor ACE2 leads to conformational change of the S2 subunit from the pre-fusion into the post-fusion state and to cleavage of the two subunits S1 and S2 by host cell proteases. The cleavage site is located at the interface between the S1 and S2 subunits and this subunit cleavage is essential for host and viral membrane fusion [15].

The N-protein is essential for viral RNA packaging. The complex of RNA and nucleocapsid is termed ribonucleocapsid. At the two ends of the N-protein, the N-terminal RNA binding domain (N-NTD) and the C-terminal dimerization domain (N-CTD) are located. The N-NTD binds to the viral RNA and the N-CTD is crucial in the packaging of the RNA by forming fibril structures [20].

The M-protein is the most abundant protein of the four structural viral proteins and a transmembrane glycoprotein with three domains: the N-terminal glycosylated ecto-domain, three transmembrane helices (TMH1-TMH3) and the C-terminal endo-domain. By interaction with S-, E- and N- proteins, the M-protein enables virion assembly and budding. Furthermore, the M-protein is involved in ribonucleocapsid formation and defines the shape of the viral envelope by bending the membrane [11, 15].

The E-protein is also a transmembrane structural protein containing three domains, the N-terminal hydrophilic ecto-domain, a hydrophobic transmembrane domain (TMD) and a hydrophilic C-terminal endo-domain with ion channel activity. It is engaged in viral assembly and budding [11, 15]. Detailed functions of the structural protein domains, however, need to be further elucidated.

1.1.3 SARS-CoV-2 cell entry

The high affinity binding of the SARS-CoV-2 RBD to the human ACE2 enables efficient cell entry and facilitates the subsequent viral spread [15]. The SARS-CoV-2 entry into the host cell is mediated by the S-protein. After the binding of the SARS-CoV-2 S protein to ACE2, initially through the S1 RBD-domain, the S-protein is cleaved by host cell proteases, such as furin, cathepsin, transmembrane protease serine 2/4 (TMPRSS2/4) and human airway trypsin-like protease (HAT), into the two functional subunits, S1 and S2 [19, 20]. This protein cleavage occurs in two steps, with the first one releasing the RBD and fusion domains and, secondly, exposing fusion peptides. These fusion peptides integrate into the host membrane and are important for the fusion of the host and virus membranes. Following, ACE2 is cleaved by polypeptides upon the binding of S1, which facilitates viral entry into the host cell. Following membrane fusion, funnel-like structures are formed by HRs, which enables the release of the viral RNA into the host cells' plasma [24].

ACE2 is highly expressed on epithelial cells from the respiratory tract, on myocardial cells, ileal epithelial cells, oesophagus epithelial cells, kidney proximal tubule cells and bladder urothelial cells and SARS-CoV-2 may thus enter these cells. Cells derived from stomach, liver and muscular samples are seen as low risk for SARS-CoV-2 infection with low ACE2 expression [25].

1.1.4 SARS-CoV-2 replication cycle

Upon binding of SARS-CoV-2 to a target cell and viral entry, viral RNA is released into the host cells' cytoplasm. Immediately after the release, the viral positive sense RNA genome is translated into viral proteins by the host cells' ribosomes, which are then cleaved into non-structural proteins, such as components of the viral RdRp. The viral positive single-stranded RNA is transcribed into a negative sense RNA, which can be replicated into new viral genome or subgenomic RNA by the viral RdRp, which is then translated into the four structural S, E, M and N-proteins as well as further accessory proteins. The N-protein, together with the newly

replicated positive sense RNA, forms the nucleoprotein complex. S-, E- and M- proteins first enter the endoplasmic reticulum (ER). Following, they are transported together with the nucleoprotein to the ER-Golgi intermediate compartment (ERGIC) for virion assembly and maturation in golgi vesicles. The progeny virus particles are then released by fusion of the vesicle with the host cell membrane via exocytosis (Figure 3) [10, 11].

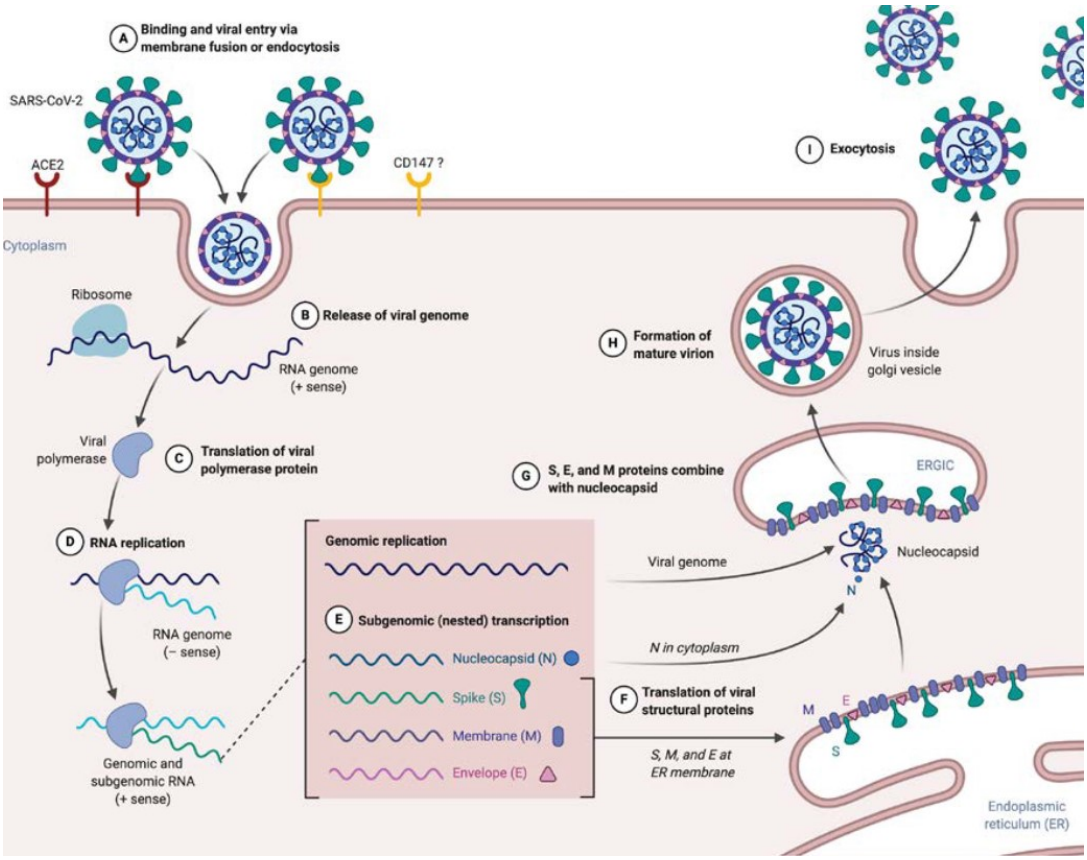

Figure 3: SARS-CoV-2 life cycle from binding of the virus to a target cell expressing ACE2 and the release of viral genome, translation of viral polymerase proteins, RNA replication, subgenomic transcription, translation of structural proteins, combination of S, E and M with nucleocapsid, formation of mature virion and, lastly, to the exocytosis of newly formed virus particles [Figure modified from Lebeau et al. [26]].

1.1.5 SARS-CoV-2 VOCs

Coronaviruses show in general a wide genomic diversity through genetic recombination and variations [27]. The genome of SARS-CoV-2 is continuously altered via the accumulation of single nucleotide polymorphisms (SNP). Nucleotide substitutions may happen frequently due to an error-prone viral RNA-dependent RNA polymerase and the subsequent natural selection of fitter SARS-CoV-2 strains. Although the SARS-CoV-2 exonuclease possesses a 3’ to 5’ proofreading function, which may reduce these high error rates, decisive point mutations may still happen [15, 16]. However, only a small proportion of these mutations indeed has an

influence on viral functions and may increase its infectivity, transmission, immune escape, pathogenicity and fitness. New SARS-CoV-2 variants, which highly impact the transmissibility, disease severity or immune evasion were classified by the WHO as ‘variants of concern’ (VOC) [30].

Especially, changes in the SARS-CoV-2 S-protein are of interest, as they possibly lead to reduced viral neutralization and to an increased transmissibility and virulence. Importantly, SARS-CoV-2 genome changes may dramatically complicate the efficiency of COVID-19 vaccines [15, 16].

The features of the, at the time of writing (17.12.2021), classified SARS-CoV-2 VOCs are listed in table 1 [26, 27].

Table 1: SARS-CoV-2 VOCs Alpha, Beta, Gamma, Delta and Omicron with molecular and clinical characteristics (17.12.2021). Changes of new variants posing high to very high risk in grey [Table created based on WHO (COVID-19) Homepage, Rambaut et al., Campbell et al., Collier et al. and Kandeel et al. [4, 33–36]].

WHO Label	PANGO Lineages	First Outbreak	Designated VOC (Earliest Sample)	Notable Mutations	Increased Transmis-sibility	Increased Hospitali-zation	Increased Mortality	Neutralising antibody activity (natural infection)	Neutralising antibody activity (vaccination)
Alpha	B.1.1.7	United Kingdom	18 Dec 2020 (Sep 2020)	69-70del, N501Y, P681H	+29%	+52%	+59%	Minimal Reduction	Minimal Reduction
	B.1.1.7 with E484K		5 Feb 2021 (Jan 2021)	E848K, 69-70del, N501Y, P681H				Considerably Reduced	Considerably Reduced
Beta	B.1.351	South Africa	14 Jan 2021 (May 2020)	K417N, E484K, N501Y	+25%	Under Investi-gation	Possibly Increased	Reduced	Efficacy retained (severe disease)
Gamma	P.1	Brazil	15 Jan 2021 (Nov 2020)	K417T, E484K, N501Y	+38%	Possibly Increased	+50%	Reduced	Retained by many
Delta	B.1.617.2	India	6 May 2021 (Oct 2020)	L452R, T478K, P681R	+97%	+85% (relative to Alpha)	+137%	Reinfections happened	Efficacy reduction for non-severe disease
Omicron	B.1.1.529	South Africa	26 Nov 2021 (Nov 2021)	P681H, N440K, N501Y, S477N, many others	Possibly Increased	Under Investi-gation	Under Investi-gation	Reduced	Efficacy reduction for symptomatic disease

Abbreviations**: PANGO**: Phylogenetic Assignment of Named Global Outbreak.

1.2 COVID-19

COVID-19 mainly affects the respiratory tract, as SARS-CoV-2 is usually transmitted through respiratory droplets and primarily infects epithelial cells from the upper and lower respiratory tract, including the lung [4, 22]. The disease outcome is very heterogeneous and can range from asymptomatic or mild flu-like symptoms as cough, sore throat and fever, to severe pneumonia and respiratory failure, including death [37]. The most common clinical manifestations of COVID-19 include fever, dry cough, fatigue, sore throat, shortness of breath, loss of the sense of smell and taste, muscle ache, atypical pneumonia and in severe cases acute respiratory distress syndrome (ARDS) [2, 4, 5].

Between 15.6% and 30.8% of SARS-CoV-2 infections may be asymptomatic with patients showing a positive result of the reverse transcription polymerase chain reaction (RT-PCR), but no clinical symptoms [32–34]. However, studies about the percentage of asymptomatic infections report very diverse results, as the number of undetected cases is usually high [42]. Of all symptomatic COVID-19 patients in the United States, 81% show a mild course of disease, while 19% of COVID-19 patients require hospitalization [43]. This hospitalization rate was calculated based on data of 1.482 hospitalized patients in 14 U.S. states and the COVID-19 U.S. surveillance (Coronavirus Disease 2019–Associated Hospitalization Surveillance Network) during March 1-28, 2020, representing numbers that apply to the SARS-CoV-2 wild type strain [43]. Hospitalization rates generally depend on the age of patients infected with SARS-CoV-2 with 2.5% in the young cohort (aged 18-49), steadily increasing to 17.2% for the elderly aged 85 or older [43]. At the time of writing (14.12.2021), the worldwide case mortality rate was 1.97%, based on the current numbers of SARS-CoV-2 confirmed cases and deaths [4].

The incubation period from SARS-CoV-2 infection to showing the first symptoms is on average 5 days [44], but it may differ from 4.5 to 15.6 days [44]. The median time interval from symptom onset to hospital admission in severe cases is 7 days, ranging from 3 to 9 days [43].

One increasing recognized problem after SARS-CoV-2 infections is termed “long COVID”. Clinical manifestations are a long-lasting disease state with debilitating symptoms, such as chronic fatigue, weakness, cough, headache, shortness of breath, myalgia and tachycardia [45]. A recently published study from Mandal et al. including 384 hospitalized COVID-19 patients demonstrated that more than 50% of COVID-19 patients still complained about

fatigue and breathlessness with signs of lung fibrosis after a median of 54 days post hospital discharge [46]. Importantly, “long COVID” can also occur after a mild course of disease in young patients [45]. Dennis et al. found that almost 70% of non-hospitalized, young, low-risk COVID-19 patients showed symptoms of “long COVID” four months after initial symptom onset in a study with 201 participants (mean age: 44) [47].

1.2.1 Mild and severe acute COVID-19

Commonly, the course of COVID-19 is graded based on disease severity into mild, moderate and severe. Mild COVID-19 is usually defined as home quarantine, while moderate or severe cases require the treatment in a hospital or on the intensive care unit (ICU), respectively [16]. Gao et al. suggested five different types of COVID-19 severity based on WHO guidance, which are asymptomatic, mild, moderate, severe and critical. More precisely, patients with an asymptomatic SARS-CoV-2 infection show no COVID-19 symptoms. Mild COVID-19 cases are characterised by mild symptoms, such as fever, fatigue, cough, muscle pain, sore throat and headache. Patients with moderate COVID-19 show mild pneumonia manifestations in lung computed tomography (CT) images. Clinical characteristics of severe COVID-19 are respiratory infection symptoms, possible shortness of breath, oxygen saturation below 93% and severely progressed lesions in chest imaging [41, 42]. Chest CT images of patients with severe COVID-19 often showed ground-glass opacities due to infection, inflammation and pneumonia [50]. Disease manifestations such as respiratory failure, need for mechanical ventilation, organ failure, shock, rapid disease progression and ARDS are seen in patients with critical COVID-19. These patients require the treatment on an ICU [48]. The causes of death following a SARS-CoV-2 infection are mainly respiratory failure, septic shock or multiple organ system failures [50].

Especially, older people (increasing risk >50 years, high risk >85 years [51]) and people of all ages with comorbidities such as hypertension, chronic obstructive pulmonary disease, diabetes, obesity, cardiovascular disease or patients under immune suppression are more susceptible to severe manifestations [49] and show higher COVID-19 mortality [2]. Furthermore, gender-based differences in the COVID-19 severity were found. The evaluation of a big data set from five European countries and China revealed that males are 50% more likely to have a serious course of COVID-19 with the requirement of hospitalization than females [52]. Males are also at 4-fold higher risk of needing ICU care than females, as identified

based on a retrospective analysis of the data of 1591 ICU patients in the Lombardy Region in Italy [53]. Based on data from 17 million patients in the UK published on the OpenSAFELY platform, males were defined to have a 57% higher risk to die with or from COVID-19 than females [54].

Severe COVID-19 is hallmarked by a deviant innate immune response with decreased antiviral interferon beta (IFN-β) levels [55], increased oxidative stress, less effective macrophages and increased pro-inflammatory cytokine and chemokine levels. Such exuberant and imbalanced immune responses with high levels of pro-inflammatory cytokines are a great risk factor for severe COVID-19 [45]. Levels of pro-inflammatory cytokines, such as interleukin (IL)-2, IL-7, IL-12 and tumor-necrosis factor alpha (TNF-α) and chemokines, such as interferon gamma-induced protein 10 (IP-10), monocyte chemoattractant protein-1 (MCP-1) and macrophage inflammatory protein-1 alpha (MIP-1α), are elevated in patients with severe COVID-19 treated on the ICU, of which 85% were affected by ARDS, as seen in a study with in total 41 hospitalized patients in Wuhan, China [56]. Additionally, inflammatory cytokine levels, such as Il-6, IL-8, IL-10 and TNF-α, were significantly elevated in severe cases of hospitalized COVID-19 patients, who suffer from respiratory distress and an oxygen saturation ≤ 93%, compared to hospitalized COVID-19 patients with less severe disease. In total 452 patients were involved in this study by Qin and colleagues [57]. Thus, hyperinflammation and an excess of pro-inflammatory cytokines may be associated with ARDS and severe COVID-19 [12, 14]. ARDS is marked by a sudden onset of inflammation in the lung, leading to respiratory failure [59]. The main contributor to high levels of pro-inflammatory cytokines are neutrophils. Regarding severe COVID-19, it is known that the number of blood neutrophils is increased, compared to patients with mild COVID-19 [60]. High neutrophil counts and at the same time low lymphocyte counts are linked to severe COVID-19 manifestations, as shown in a meta-analysis by Lagunas-Rangel et al. based on five studies regarding the neutrophil-to-lymphocyte ratio in severe and mild COVID-19 [59]. Such high neutrophil counts are a hallmark for inflammation and reflect a dysregulated and exuberant immune response, leading to hyperinflammation and a severe course of COVID-19 [43, 59]. Although lymphocyte counts are decreased in patients with severe COVID-19, these cells may be highly activated. Especially, NK cells show an activated effector phenotype, leading to increased levels of inflammatory cytokines, which thus also contribute to hyperinflammation and COVID-19 progression [61].

In contrast, especially children and adolescent mostly show a very mild or asymptomatic course of disease, which goes along with higher serum levels of the pro-inflammatory cytokine IL-17A, compared to older patients [62]. These findings suggest that distinct cytokines and a more robust and regulated innate immune response may be protective against severe COVID-19 [62].

1.2.2 COVID-19 treatment and vaccines

For the treatment of severe COVID-19, several widely used antiviral drugs are applied, often off-label. At the time of writing (14.12.2021) the treatment with Remdesivir and Tocilizumab has been authorised by the European Medicines Agency (EMA) in the European Union (EU) for the use in COVID-19 patients, who require supplemental oxygen due to severe pneumonia [63]. Remdesivir is a viral RNA polymerase inhibitor, which interferes with the transcription of new viral RNA, and thus prevents the virus from reproducing inside the host's cells [63]. Tocilizumab is an antagonistic monoclonal antibody, which binds and blocks the receptor for IL-6 and, subsequently, reduces inflammation [63]. Additionally, patients who do not require supplemental oxygen may be treated with Regdanvimab and Casirivimab/Imdevimab, which are monoclonal antibodies that bind to the SARS-CoV-2 S-protein and thereby prevent the virus from entering the host's cells [63].

At the time of writing (14.12.2021), four COVID-19 vaccines have been authorised for use by the EMA in the EU: the two mRNA vaccines BNT162b2 (BioNTech/Pfizer) and mRNA-1273 (Moderna) and the two vector-based vaccines ChAdOx1-S (Oxford/AstraZeneca) and JNJ-78436735 (Janssen) [26, 51]. All of these four approved vaccines are based on the SARS-CoV-2 S-protein, either as mRNA, or as a gene inserted into a viral adeno vector, both function as template for the production of the S-protein [64]. The main focus of the COVID-19 vaccine development lay on the prevention of severe manifestations with requirement for hospitalization or intensive care. The six clinical endpoints for evaluating COVID-19 vaccine efficacy, suggested by Mehrotra et al., are SARS-CoV-2 infection, symptomatic COVID-19, asymptomatic infection, severe COVID-19, non-severe COVID-19 and burden of disease [65].

The mRNAs of both the mRNA-1273 and BNT162b2 vaccines are engulfed by a lipid nanoparticle and encode for the SARS-CoV-2 full-length S-protein in the pre-fusion state [64, 65]. After administration, the mRNA is translated into the SARS-CoV-2 S-protein by the cellular

translation machinery. The immune system reacts to this foreign protein by producing S-protein-specific antibodies as well as S-protein-specific CD4+ and CD8+ T cells [64]. Polack and colleagues conducted an observational *in vivo* study with 43,548 BNT162b2 vaccinees and the primary endpoints were the efficacy against COVID-19 and the efficacy in patients with and without prior infection. Secondary endpoints were the prevention of severe COVID-19. The authors showed that the BNT162b2 mRNA vaccine has an efficacy of 95% after 7 days after the second dose with rare cases of adverse events after vaccination. The prevention of severe COVID-19 was shown to be effective: 9 patients in the placebo group came down with severe COVID-19 and only one patient in the vaccinated group showed severe COVID-19 symptoms after the first BNT162b2 dose, none after the second dose [66]. The mRNA-1273 vaccine functions according to the same principle as BNT162b2 [68]. The primary endpoint of the mRNA-1273 vaccine was based on confirmed COVID-19 two weeks after the second dose and prevention of symptomatic COVID-19. The secondary endpoint aimed to avoid severe COVID-19 [69]. A trial with 30,000 participants revealed a vaccine efficacy of 94.1% after two mRNA-1273 doses [68], with severe COVID-19 cases only occurring in the placebo group [69].

Concerning the viral vector vaccines ChAdOx1-S and JNJ-78436735, the gene with the information of the SARS-CoV-2 S-protein migrate into the human cell via a modified Adenovirus, which serves as a vector. The Adenovirus vector with the included S gene enters the cell via endocytosis and is translated into the S-protein, which is then recognized by the immune system [64]. Endpoints of the ChAdOx1-S vaccine were prevention of symptomatic COVID-19 and severe disease [70]. For the ChAdOx1-S vaccine, the efficacy was 60% in a clinical trial with 24,000 participants [64]. Additionally, overall safety and beneficial reactogenicity were observed [70]. Endpoints of JNJ-78436735 were prevention of moderate and severe COVID-19 14 and 28 days post vaccination [71]. For JNJ-78436735, the efficacy was 67% in a trial with 44,000 participants 28 days following vaccination [64]. The studies of all vaccines pledge vaccine efficacy and protection against severe COVID-19 across sex, age and geographies [65, 68–70].

1.3 NK cell response

1.3.1 NK cells in viral infections

Natural killer (NK) cells are in general important effector cells in the interface of the innate and adaptive immune responses. Importantly, NK cells do not need a prior antigen sensitization, which enables them to respond to virally infected cells early in innate immune responses [72]. They are thus crucial in the first-line defense against distinct acute viral infections [73]. Crucially, NK cells are able to distinguish virally infected cells from uninfected cells with diverse surface receptors that act as activating or inhibitory receptors. Following, NK cells are able to tolerate healthy 'self-cells', while attacking stressed or virally infected cells [74].

NK cells can be activated by several pro-inflammatory cytokines such as IL-2, IL-12, IL-15 and IL-18 as well as type I IFN [72]. These cytokines are produced in response to viral pathogen-associated molecular patterns (PAMPs) sensed by the host cell pattern recognition receptors (PRRs) [45]. Following activation, NK cells produce cytokines, such as IFN-γ, TNF-α and granulocyte/macrophage colony-stimulating factor (GM-CSF) [72]. IFN-γ is crucial in the early control of infections by affecting innate immune cells and later on by influencing adaptive immune responses. Regarding innate effects, IFN-γ activates macrophages, which leads to enhanced pathogen killing. Additionally, IFN-γ acts activating on adaptive immune cells, such as dendritic cells (DCs) and CD4+ T cells. TNF-α and GM-CSF also activate macrophages [75]. In addition, NK cells produce high amounts of chemokines, such as MIP-1α, MIP1-β and the CC-chemokine ligand 5 (CCL5) [72], which play an important role in early antiviral defense by recruiting macrophages and impact adaptive responses by activating distinct T cell subsets [75]. These soluble factors are all crucial in haematopoiesis as regulators and influence subsequent cellular networks [72].

Human NK cells can be divided into the two main subsets $CD56^{dim}$ and $CD56^{bright}$ NK cells, with the subclasses $CD56^{dim}$ $CD16^{+}$, $CD56^{dim}$ $CD16^{-}$, $CD56^{bright}$ $CD16^{+}$ and $CD56^{bright}$ $CD16^{-}$. The larger fraction, over 90% of NK cells in the peripheral blood and spleen, are $CD56^{dim}CD16^{+}$ NK cells. This NK cell subset is the main contributor to the NK cell-mediated cytotoxicity, while $CD56^{bright}CD16^{-}$ NK cells are less cytotoxic. Instead, $CD56^{bright}CD16^{-}$ NK cells have a specialized role in the production of cytokines, such as IFN-γ, upon stimulation with ILs [74].

The two main effector functions of NK cells are cytotoxicity and the release of pro-inflammatory cytokines in the antibody-dependent cellular cytotoxicity (ADCC). Amongst other activating receptors, NK cells express the low-affinity Fcγ receptor IIIa (FcγRIIIa/CD16A) that enables the detection of antibody-opsonized infected cells, cell free virions and antigens in the ADCC response [74]. Upon interaction of the FcγRIIIa on NK cells and the fragment crystallisable (Fc) domain of antibodies that are bound to antigens on an infected cell [76], cytolytic proteins, such as perforin and granzyme are released, which induce the apoptosis of virally infected target cells and thus limit viral dissemination [74]. The serine protease granzyme and the cytolytic protein perforin are released from NK cells by granule exocytosis and then disrupt the membranes of the target cells causing cell death [77]. Thereby, perforins form pores into the target cell, so granzymes can gain entry into the cell's cytosol and, subsequently, cause apoptosis, with granzyme b being, amongst others, the strongest apoptosis-inducer [78]. Additionally, cytokines, such as IFN-γ and TNF-α are released by NK cells in the ADCC response against infected cells. IFN-γ is then involved in the maturation of DCs, in the priming of $CD4^+$ T cells and may influence adaptive immune responses by directly acting on T and B cells. TNF-α also promotes the maturation of DCs and impact adaptive responses [74]. These NK cell effector functions in ADCC, such as the production of cytokines and lysis of virus-infected cells are crucial in the first-line defense in viral, bacterial and parasitic infections and were shown to reduce disease severity in respiratory syncytial virus (RSV), parainfluenza virus (PIV) and influenza A virus (IAV) infections in mice and hamsters [72]. However, an excessive NK cell activation in ADCC, and, thus, increased IFN-γ and TNF-α production and cell killing, may lead to increased lung inflammation and organ injury [72], as recently demonstrated for IAV and RSV infection [59, 60]. Especially in respiratory infections, the extensive killing of infected lung epithelial cells by NK cells in cytolytic responses was shown to excel the regenerative rate of lung cells and may lead to lung injury [72]. Li an colleagues investigated acute lung immune injuries in RSV infections and found out that the overall counts of NK cells and, especially, levels of strongly activated NK cells in the lung are significantly increased in RSV-infected mice compared to control mice. This makes NK cells the possible contributor to virus- and immune system-induced lung injury [79].

1.3.2 NK cells in COVID-19

In SARS-CoV-2 infections, the importance of NK cells was recently demonstrated in a study of 204 hospitalized COVID-19 patients, which showed lower NK cell counts in patients with severe course of COVID-19, compared to hospitalized patients with less severe COVID-19 [81]. A study by Maucourant and colleagues involving 17 patients with severe COVID-19, 10 patients with moderate COVID-19 and 17 healthy individuals showed that both $CD56^{bright}$ and $CD56^{dim}$ NK cell counts were significantly decreased in patients with moderate and severe COVID-19 compared to the control cohort [61]. Overall it is evident that NK cell counts are significantly reduced during SARS-CoV-2 infections in critically ill patients compared to patients with mild COVID-19, indicating that NK cells are crucial in viral clearance and in modulating immune responses [53, 63]. These lower NK cell counts may lead to the reduced clearance of SARS-CoV-2 and high SARS-CoV-2 viral loads, which are further associated with an increased tissue damage [83]. Low circular NK cell counts may however be associated with the sequestration of the cells to the lung [72]. Liao et al. detected for example higher levels of NK cells in BALF samples of COVID-19 patients, which would indicate a sequestration of immune cells from the blood to the lung [84].

Although NK cell counts are reduced in patients with severe COVID-19, they show a highly activated phenotype in both moderate and severe COVID-19, as demonstrated by a recently published study by Maucourant and colleagues. A principal component analysis (PCA) of protein expression phenotypes of $CD56^{bright}$ and $CD56^{dim}$ NK cells revealed that NK cells in the blood of patients with both moderate and especially severe COVID-19 show an activated effector phenotype with high expression of perforin and granzyme b [61], which may contribute to inflammation and tissue damage [83]. The same study group could also detect these activated NK cells in BALF samples of patients with moderate and severe COVID-19 [61]. The high-level activation of NK cells may also be associated with the release of high levels of pro-inflammatory cytokines, such as IFN-γ and TNF-α, which may be associated with tissue damage [83].

Patients with severe COVID-19 show NK cells with an exhausted phenotype that could be associated with the repeated stimulation of highly activated NK cells [83]. This was shown in mice during respiratory infections, where increased lung injury and inflammatory status were detected due to a heightened extent of NK cell activation and increased IFN-γ levels [72]. Also

in SARS-CoV-2 infections, the elimination of infected airway epithelial cells due to the NK cell production of cytolytic proteins may be greater than the regenerative capacity of these cells, resulting in the damage of lung tissue [72].

Clearly, the role of NK cells in the immunopathogenesis of COVID-19 is so far controversial, because it is unclear how the reduced numbers of NK cells and at the same time the persistence of highly active NK cells resulting in high levels of IFN-γ, TNF-α, granzyme and perforin is involved in disease progression and increased organ damage in patients with severe COVID-19.

1.3.3 FcγRIIIa-158 SNP

The FcγRIIIa is encoded by the *FCGR3A* gene, which is highly expressed on NK cells and, to a lesser extent also on neutrophils, macrophages and monocytes [85] and distinct T cell subsets [86]. *FCGR3A* encodes for an important SNP termed rs396991 (T/G) at the amino acid position 158. This SNP results either in the expression of the amino acid phenylalanine (F) due to the presence of the nucleobase thymin (T) or the amino acid valine (V) due to the presence of the nucleobase guanine (G). The three resulting variants, the homozygous T/T (F/F) variant, the heterozygous T/G (F/V) variant and the homozygous G/G (V/V) variant are known to have different binding affinities to IgG antibodies. Whereas the FcγRIIIa-158-V/V, is described as a high affinity variant, the FcγRIIIa-158-F/F shows a significant lower affinity to IgG antibodies [87]. The affinity of FcγRIIIa-158-V/V is at least two-fold greater than FcγRIIIa-158-F/F and, consequently, may lead to the induction of stronger NK cell effector functions [70, 71]. In monoclonal antibody therapies, such as infliximab and rituximab, the high-affinity FcγRIIIa-158-V/V resulted in higher response to the therapy and higher extent of antibody-mediated ADCC [27, 28], as shown in a study by Weng et al. in 87 patients with follicular lymphoma [90]. The role of the heterozygous FcγRIIIa-158-F/V variant in the extent of NK cell activation is not clearly defined. A study by Talathi and colleagues showed that the NK cell activation in human immunodeficiency virus (HIV)-specific and IgG-dependent ADCC is significantly higher with the FcγRIIIa-158-V/V variant compared to both FcγRIIIa-158-F/V and FcγRIIIa-158-F/F [91]. Koene et al. showed, however, an intermediate affinity of the heterozygous FcγRIIIa-158-F/V to IgG3 antibodies compared to high-affinity FcγRIIIa-158-V/V and low-affinity FcγRIIIa-158-F/F [92]. In contrast, Ruyssen-Witrand et al. suggested differing between patients with one or two copies of the V allele (FcγRIIIa-158-F/V and FcγRIIIa-158-V/V) and the homozygous FcγRIIIa-

158-F/F variant, directing the attention on the V allele that is supposed to be responsible for high-affinity receptor variants. The study by Ruyssen-Witrand et al., involving 111 patients with rheumatoid arthritis treated with rituximab, showed that patients carrying at least one V allele showed a higher response to rituximab due to a higher affinity to the antibody than patients with the FcγRIIIa-158-F/F variant [93]. However, in a study with 303 patients with Guillain-Barré syndrome (GBS), the heterozygous FcγRIIIa-158-F/V variant was seen to be associated with severe GBS compared to the low affinity FcγRIIIa-158-F/F that was linked to the mild form of GBS [94].

1.4 Antibody-mediated responses to SARS-CoV-2

Antibodies play a crucial role in both innate and adaptive immunity and in virus defense, as they block viral cell entry and replication and are relevant in effector functions. Neutralizing antibodies are in general crucial for virus clearance, for blocking viral infection and for protection against viral disease. Neutralizing antibodies are induced in response to natural infections or vaccinations and they hallmark SARS-CoV-2 immunity [95, 96]. Non-neutralizing antibodies mediate antibody-dependent effector functions [97].

In response to an infection with SARS-CoV-2, SARS-CoV-2-specific IgM, IgG and IgA antibodies are produced and secreted by plasma cells. IgM and IgG antibodies are the highest in the plasma, whereas IgA antibodies are mainly present in secretions, such as the saliva [98] and, hence crucial in the mucosal anti-viral immunity [99]. SARS-CoV-2-specific IgM and IgA antibodies peak early during infection and are transient. IgM and IgA levels are the highest during acute infections and are low in convalescent plasmas. SARS-CoV-2-specific IgM antibodies peak after 16 to 30 days [100], in other studies between 20 and 22 days post symptom onset [99]. Following, IgM levels decrease steadily until only 25% of the maximum IgM antibody levels are detectable after 115 days post symptom onset, as described in a study by Isho and colleagues involving 128 COVID-19 patients with a follow-up of 115 days post symptom onset [100]. Consequentially, high IgM levels mark a relatively recent infection [100].

IgA is overall the most abundant isotype in the human body and can mainly be detected in mucosal tissues. Plasma IgA may induce pro-inflammatory and effector responses. IgA can be

divided into the two subclasses IgA1 and IgA2, which have different hinge regions, glycosylation profiles and effects on immune cells [101]. In secretions, IgA1 and IgA2 can be found in same amounts, but IgA1 is found in higher levels in plasma compared to IgA2. IgA2 induces higher levels of effector functions than IgA1 and has stronger pro-inflammatory effects due to a different glycan composition [101]. In SARS-CoV-2 infections, SARS-CoV-2-specific IgA levels peak after 16 to 30 days post symptoms onset, followed by a steady decline afterwards. At day 115 anti-RBD IgA antibody levels are reduced by 84.2% [100].

In contrast, IgG antibodies peak later during SARS-CoV-2 infections and are long-term detectable in convalescent COVID-19 patients, with IgG levels being often higher in convalescent plasma than in the plasma during the acute SARS-CoV-2 infection [100]. The median time of IgG seroconversion is 17 to 19 days after symptoms onset [99]. Anti-SARS-CoV-2 RBD-specific IgG levels then peak after 31 to 45 days after symptoms onset, anti-SARS-CoV-2 S-specific IgG levels peak after 61 to 75 days post symptoms onset and persist in the plasma for at least 115 days after symptom onset [100]. The isotype IgG is the most abundant one in human plasma with four subclasses IgG1, IgG2, IgG3 and IgG4, named in order of decreasing abundance (60%, 32%, 4%, 4%, respectively) [102]. The different IgG subclasses show differences in antigen binding, immune complex formation triggering effector cells and half-life [102]. The difference in the affinities of the IgG subtypes is due to different amino acid sequences in the constant region [103]. Importantly, the two subtypes IgG1 and IgG3 are the most important subtypes in most viral infections. IgG1 and IgG3 trigger potent non-neutralizing effector functions in SARS-CoV-2 infections, as they both show high affinity to the FcγRIIIa, with highest affinity of IgG3, and second highest of IgG1, compared to IgG2 and IgG4 with very low affinity [102]. In SARS-CoV-2 infections, IgG2 and IgG4 are overall less relevant, as IgG2 responses to bacterial infections and IgG4 plays a major role in allergies [102]. Therefore, IgG1 and IgG3 are the most important IgG subtypes for the SARS-CoV-2-specific ADCC response [76]. IgG1 is the most prominent subclass in the plasma and most important in the antibody response to SARS-CoV-2 antigens. The IgG1 antibody response is mainly directed against foreign proteins, and to lesser extent to polysaccharides and allergens [102]. IgG3 antibodies are mainly directed against foreign antigens and crucial for complement activation. IgG3 antibodies are the main inducers of pro-inflammatory effector functions due to the high affinity to FcγRs, which may result in excessive inflammatory responses. Furthermore, IgG3 antibodies are detected considerably earlier compared to IgG1 in viral

infections, allowing an early onset of non-neutralizing effector responses [102]. IgG1 and IgG3 antibodies differ structurally especially in their length and number of disulphide bridges in the hinge region connecting two heavy chain-light chain heterodimers and in the N-terminal CH2 domain, which mediates complement component 1q (C1q) and FcγR binding [102].

In SARS-CoV-2 infections IgM, IgG and IgA are mainly directed against the SARS-CoV-2-encoded N- and S-protein [98]. S-protein-specific IgM, IgG and IgA antibodies may prevent the virus from binding to subsequently infecting a host cell. Whereas most studies focus on antibodies directed against the S-protein in regard of neutralizing activity, Weisberg et al. detected IgG antibodies directed against the SARS-CoV-2-specific N-protein, which is essential for viral replication [98]. Zhou et al. and Ni et al. could also detect IgM antibodies directed against the N-protein [98, 99]. Isho et al. showed the longitudinal profile of SARS-CoV-2 N-directed IgM, IgG and IgA antibodies in the plasma. The pattern is similar to S-directed antibodies with a peak at 16-30 days post symptom onset and a subsequent decrease of IgM and IgA antibodies, but steady levels of IgG antibodies until at least 115 days post symptom onset [100].

Non-hospitalized and hospitalized COVID-19 patients show generally different SARS-CoV-2-specific antibody titres. In the plasma of patients with severe COVID-19, antibody titres are in general higher compared to mild COVID-19 [100–102]. A recently published study demonstrated that a strong SARS-CoV-2-specific IgM, IgG and IgA antibody response is mainly detectable in hospitalized COVID-19 patients with severe symptoms [100]. Cervia et al. compared antibody levels in 26 patients with mild COVID-19 and 38 patients with severe COVID-19. In patients with mild COVID-19, IgA levels were low or even absent and IgG seroconversion could be detected in most of the non-hospitalized patients after 12 to 14 days post symptoms onset. Both plasma IgA and IgG antibody levels directed against SARS-CoV-2-specific S1 were significantly higher in patients with severe COVID-19 compared to mild COVID-19 and could be detected earlier during the disease, at 3 to 5 days after symptom onset. Interestingly, high SARS-CoV-2-specific IgA levels in the plasma were linked to severe ARDS, as stated by Cervia et al. [106]. Overall, studies showed that SARS-CoV-2-specific IgG seroconversion can be detected in the plasma of at least 90% of COVID-19 patients [62], whereas the IgG1 and IgG3 isotypes are most frequent [105].

1.4.1 Non-neutralizing antibodies in SARS-CoV-2 infection

Besides the neutralizing antibody response, antibodies may also mediate non-neutralizing effector functions [97]. SARS-CoV-2-specific IgG antibodies bind to SARS-CoV-2 antigens with the variable fragment antigen-binding (Fab) domain and activate effector cells via the interaction of the constant Fc domain with FcγRs, which are expressed on effector cells [97].

Non-neutralizing antibodies play a role in antibody-dependent effector functions, such as ADCC, antibody-dependent cellular phagocytosis (ADCP), antibody-dependent complement deposition (ADCD) and complement-dependent cytotoxicity (CDC) [36, 37]. These effector functions are crucial in viral clearance, but they may also exacerbate inflammation. Adeniji and colleagues investigated the role of anti-SARS-CoV-2 S-specific IgG antibodies in these different effector functions in 60 COVID-19 patients, 40 hospitalized and 20 non-hospitalized. In brief, IgG antibodies from hospitalized COVID-19 patients led to higher ADCD, and, thus, higher systemic inflammation, but lower ADCP, compared to antibodies of patients with mild COVID-19. In the non-severe cohort, ADCP responses were higher, which resulted in lower inflammation [110]. Concerning ADCC, anti-SARS-CoV-2 RBD-specific IgG antibodies from hospitalized patients elicited significantly higher ADCC compared to non-hospitalized patients. However, anti-SARS-CoV-2 S1-specific IgG antibodies showed conversely significantly higher ADCC responses in non-hospitalized, compared to hospitalized COVID-19 patients [110].

Although non-neutralizing effector functions such as ADCP, ADCC and CDC were demonstrated to have a protective role in viral infections, such as HIV and influenza viruses [111] and were furthermore associated with viral clearance and resolution of disease, there is no clear evidence for the role of non-neutralizing effector functions in SARS-CoV-2 infections [112]. Altogether, these different antibody effector mechanisms are only little investigated in SARS-CoV-2 infections and their role in COVID-19 outcome and severity remains unknown.

1.4.2 Antibody-mediated ADCC in SARS-CoV-2 infection

In the ADCC response, as illustrated in figure 4, SARS-CoV-2-specific antigens are presented on an infected cell or cell-free virions, where they are accessible for the Fc part of IgG1 and IgG3 antibodies [110]. The binding of FcγRIIIa to the Fc domain of IgG1 and IgG3 leads to the activation of effector cells [76]. These antibody-dependent effector cells in ADCC, meaning immune cells expressing FcγRIIIa, mainly include NK cells [113], and to a lower extent also

monocytes, macrophages, NKT cells or γδ T cells [114]. Upon NK cell activation, cytotoxic granules, such as perforin and granzyme b that induce killing of SARS-CoV-2 infected cells, are released. In addition, pro-inflammatory cytokines, such as IFN-γ, are secreted, which mediate subsequent adaptive immune responses [76]. Although the importance of ADCC in the limitation of distinct viral pulmonary infections, such as RSV was demonstrated [76], the impact of ADCC on COVID-19 severity has not yet been completely clarified. It is assumed that the ADCC response is crucial in controlling the spread of SARS-CoV-2, but may also lead to overshooting responses and disease progression [88].

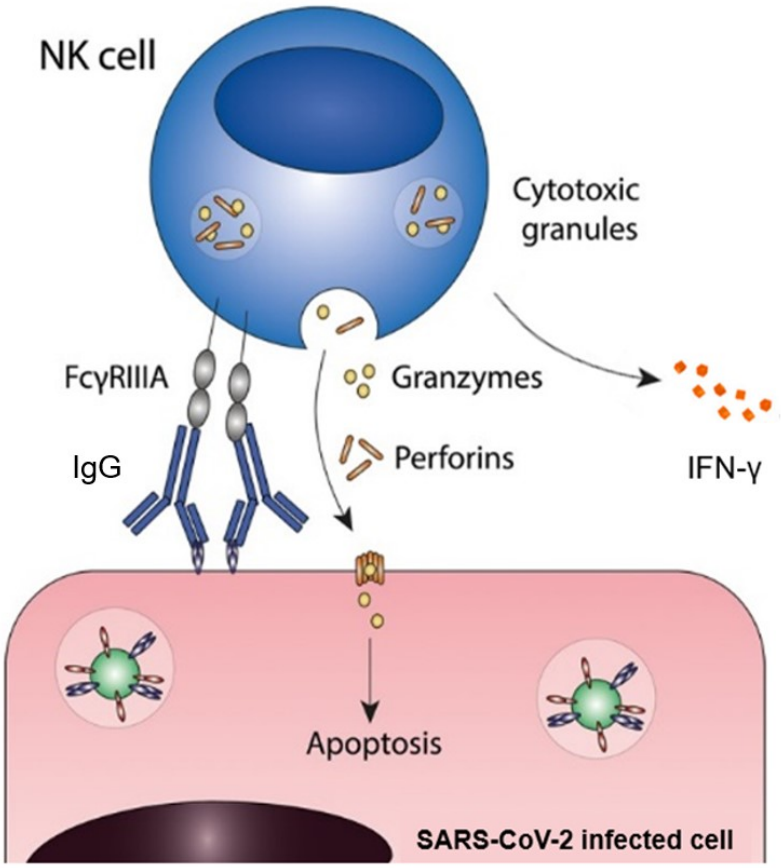

Figure 4: NK cell effector function in ADCC in SARS-CoV-2 infection: The SARS-CoV-2 infected cell presents viral antigens on its surface. IgG antibodies thus bind to the antigens with their Fab domain and interact with the FcγRIIIa of NK cells with their Fc domain [Figure modified from van Erp et al. [76]].

2. Rationale and Objectives

SARS-CoV-2 is a pandemic virus that has caused at the date of writing (14.12.2021) over 5.3 Million deaths [4]. It is thus crucial to evaluate SARS-CoV-2-specific immune responses in COVID-19 patients to define on the one hand protective immune responses, but also to identify on the other hand immune responses that may contribute to the immunopathogenesis and COVID-19 severity. NK cells are key players in the first line of the SARS-CoV-2-specific immune defense and important effector cells for mediating ADCC. The SARS-CoV-2-specific and NK cell-mediated ADCC response may contribute to the limitation of SARS-CoV-2 replication or to the pathogenesis of COVID-19 [16]. In our project, we thus focused on the fine specificity of the SARS-CoV-2-specific and NK cell-mediated ADCC response in non-hospitalized and hospitalized COVID-19 patients and aimed to analyse whether ADCC contributes to disease severity or to the clearance of SARS-CoV-2 infections.

In the first part of the project, the FcγRIIIa-158-F/F, -F/V and -V/V variants were determined by Sanger-sequencing and, subsequently, the distribution of the FcγRIIIa-158 variants were compared between non-hospitalized and hospitalized COVID-19 patients. Secondly, the effect of the three FcγRIIIa-158 variants on the SARS-CoV-2-specific ADCC responses was determined in an IgG-dependent *in vitro* $CD56^{+}CD16^{+}$ NK cell activation experiment, followed by flow cytometry. We then evaluated the overall extent of SARS-CoV-2-specific $CD56^{+}CD16^{+}$ NK cell activation in the IgG-dependent ADCC response with *in vitro* $CD56^{+}CD16^{+}$ NK cell activation assays, followed by flow cytometry and ELISpot analysis in both non-hospitalized and hospitalized COVID-19 patients. Additionally, an ELISA assay was conducted to determine the longitudinal SARS-CoV-2 N-, S1- and S2-protein-specific IgM, IgG1, IgG3, IgA1 and IgA2 antibody response in non-hospitalized and hospitalized COVID-19 patients over a period of 27 days post symptoms onset. Overall, we aimed to clarify in our study, whether the antibody-dependent NK cell response in SARS-CoV-2-specific ADCC responses is protective in SARS-CoV-2 infections or contributes to the immunopathogenesis and disease severity in COVID-19 patients.

3. Material and Methods

3.1 Study Cohort

3.1.1 Respiratory Swabs from COVID-19 patients

In total 197 Austrian COVID-19 patients (41.2 % female, median age: 59.2), who were confirmed SARS-CoV-2 positive by a recently published real-time RT-PCR [115] were included in the study. Of all 197 patients, respiratory swabs were available between 23.03.2020 and 24.04.2020, which were stored in the biobank of the Center for Virology, Medical University of Vienna, and used for the genetic analysis of the *FCGR3A* gene (Section 3.3). All patients were infected with SARS-CoV-2-wild-type, which was the dominant strain at that time in Austria. The patient cohort was divided into two different groups based on disease severity: 46 (23.4%) non-hospitalized patients with very mild symptoms who stayed in home quarantine (45.7% female, median age: 48.8) and 151 (76.6%) hospitalized patients with severe symptoms (35.8% female, median age: 62.2). The non-hospitalized cohort was significantly younger compared to the hospitalized cohort. From the 151 hospitalized COVID-19 patients, 40 were treated on the ICU. From all hospitalized patients, 34 (22.5%) deceased with COVID-19, 12 on the ICU (35.3%) and 22 on non-ICU (64.7%). Furthermore, we included 99 Austrians without any COVID-19 symptoms showing a negative SARS-CoV-2 RT-PCR result, who were tested routinely for a SARS-CoV-2 infection, as controls (47.5% female, median age: 63).

3.1.2 Plasma samples from COVID-19 patients

From our study cohort, plasma samples of in total 19 hospitalized COVID-19 patients (26.3% female, median age: 64.3) and additional 10 non-hospitalized COVID-19 cases (60% female, median age: 39.7) were available for the ELISA (Section: 3.4) and ADCC (Section: 3.5) assays. Three out of the 19 hospitalized COVID-19 patients (15.8%) required the treatment on the ICU (33.3% female, median age: 55.33). Differences regarding the gender distribution (p=0.11) and the age (p=0.89) of these two cohorts were not significant. From the hospitalized patients, sequential plasma samples for up to 27 days post symptoms onset were collected at a 2- to 3-days interval between 23.03.2020 and 24.04.2020. Additionally, six plasma samples from

SARS-CoV-2 seronegative donors were obtained from the biobank, which were taken for routine vaccination titer controls before the SARS-CoV-2 outbreak in the years 2014 and 2018.

In addition, we included 26 voluntary and healthy blood donors in our study cohort, from which $CD56^+CD16^+$ NK cells were isolated for the ADCC assays.

3.2 Ficoll-Separation and primary human $CD56^+CD16^+$ NK cell subset isolation

Freshly prepared buffy coats from healthy voluntary blood donors were provided by the Austrian Red Cross. Peripheral blood mononuclear cells (PBMCs) were first isolated by Ficoll density gradient centrifugation and the $CD56^+CD16^+$ NK cell subset was then enriched by two-step magnetic labelling following the protocol of Miltenyi Biotec (Human $CD56^+CD16^+$ NK Cell Isolation Kit). In brief, 25 ml of buffy coat was layered on 20 ml Ficoll-Paque™ PLUS (Life Science products Cytiva). For separation of the different blood components, the buffy coat-Ficoll overlay was centrifuged at 400xg for 45 min at 20°C without break. After centrifugation, plasma and PBMCs were removed for further use. The plasma was stored at -20°C for subsequent sequencing of the FcγRIIIa-158 SNP (Section: 3.3). The PBMC layer was transferred to a 50 ml falcon tube and total cell counts were counted in a hemocytometer C-Chip with Neubauer grid (NanoEntek) using trypan blue (Fluka Analytical), according to the manufacturers instruction.

For the isolation of the $CD56^+CD16^+$ NK cell subset, cells were centrifuged at 300xg for 10 minutes and the supernatant was removed. The cell pellet was resuspended in 400 µl $CD56^+CD16^+$ NK cell isolation buffer [1]. 100 µl of NK Cell Biotin-Antibody Cocktail were added and the cells were incubated for 10 minutes at 4°C. After adding additional 300 µl of cell isolation buffer, 200 µl of NK Cell MicroBead Cocktail were added and incubated for 15 minutes at 4°C. Cells were washed by adding 15 ml of $CD56^+CD16^+$ NK cell isolation buffer and centrifuged at 300xg for 10 minutes at 4°C. The supernatant was discarded and cells were resuspended in 500 µl of cell isolation buffer. For the magnetic separation, two pre-cooled LS columns were placed in a magnetic field of a suitable magnetic cell separator (MACS® Separators, Miltenyi Biotec). Columns were prepared by rinsing with 3 ml of cell isolation

[1] Cell isolation buffer: 1x PBS (0.8 g/l NaCl + 0.145 g/l $Na_2HPO_4*2H_2O$ + 0.02 g/l KCl + 0.02 g/l KH_2PO_4) + 0.5% FCS + 2 mM EDTA, pH = 7.2

buffer and, following, the cell suspension was applied onto the columns. Unlabelled $CD56^+$ NK cells pass the column and need to be collected, whereas, labelled non-$CD56^+$ NK cells remain in the columns. The columns were washed three times with 3 ml cell isolation buffer and the total effluent was collected, as it contains the pre-enriched $CD56^+$ NK cell fraction. The effluent was then centrifuged at 300xg for 10 minutes, the supernatant was removed and $CD56^+$ NK cells were resuspended in 100 µl of cell isolation buffer. 100 µl of CD16 Microbeads were added and incubated for 15 minutes at 4°C. Cells were washed by adding 4 ml of cell isolation buffer and centrifuged at 300xg for 10 minutes. The supernatant was discarded, cells were resuspended in 500 µl of cell isolation buffer and applied onto MS columns. These columns were pre-cooled at 4°C and prepared by rinsing with 500 µl of cell isolation buffer. In this step, the effluent was not collected as the labelled $CD56^+CD16^+$ NK cell subset remains in the columns. Columns were washed three times with 500 µl of cell isolation buffer. For collection of the $CD56^+CD16^+$ NK cells, the columns were removed from the magnetic field and placed on a suitable collection tube. 1 ml of cell isolation buffer was added to the columns and the fraction with the magnetically labelled cells was flushed out by firmly pushing the plunger into the column. Thus, 1 ml of $CD56^+CD16^+$ NK cells were collected, counted in a hemocytometer with trypan blue and frozen in 1 to 1.5 ml $CD56^+CD16^+$ NK cell freezing medium [2] at a concentration of 2-4x10^6 viable $CD56^+CD16^+$ NK cells per tube in a CoolCell LX Freezing Container (BioCision, Brooks Life Sciences) overnight at −80 °C.

For visualization of the $CD56^+CD16^+$ NK cell subset and to confirm the purity of this isolated subset, flow-cytometry staining was done. In brief, NK cells were removed from -80°C and thawed in a 37°C water bath for 3 minutes. Cells were centrifuged at 300xg for 5 minutes in 4 ml complete RPMI medium [3] (Sigma Aldrich) and rested overnight in complete RPMI medium with 10 ng/ml IL-12 (PeproTech Austria) and 100 ng/ml IL-18 (Biozym Scientific) at a concentration of 5x10^5 cells/ml. On the next day, cells were harvested by centrifugation at 400xg for 5 minutes in a 15 ml falcon tube, washed once with 4 ml Opti-MEM I Reduced Serum Medium (Gibco, Fisher Scientific) and resuspended in 1 ml Opti-MEM. Live cells were counted with trypan blue in a hemocytometer with Neubauer grid (NanoEntek) and diluted to get a concentration of 1x10^6 cells. 4 ml Opti-MEM were added and cells were centrifuged at 400xg for 5 minutes and the supernatant was discarded. Cells were resuspended in 100 µl of PBS,

[2] Freezing Medium: 90% FCS + 10% DMSO

[3] Complete RPMI medium: RPMI 1640 (Thermo Fisher Scientific), 10% FCS, 1% L-Glutamine

with addition of 2.5 µl of APC-H7 Mouse anti-human CD16, 10 µl of APC Mouse anti-human CD56 and 1 µl of LIVE/DEAD™ Fixable Green Dead Cell Stain and vortexed. After incubation of the cells for 20 minutes in the dark at room temperature, cells were washed by addition of 3 ml of buffer and centrifuged at 400xg for 5 minutes. The supernatant was discarded and the cell pellet was dissolved in 100 µl of FACS buffer, cells were transferred into FACS tubes (Falcon) and stored at 4°C in the dark until fluorescent analysis. The $CD56^{+}CD16^{+}$ NK cell subset was analysed with the BD FACSCanto II flow cytometer (BD Biosciences) using the BD FACSDiva Software (Version 6.1.1 and Version 9.0, BD Biosciences). Finally, data were evaluated using FlowJo (Version 10.7.2, FlowJo, BD Biosciences).

In total, we isolated the $CD56^{+}CD16^{+}$ NK cell subset from 26 different blood donors with the three different variants (9x FcγRIIIa-158-F/F, 12x FcγRIIIa-158-F/V, 5x FcγRIIIa-158-V/V).

3.3 FcγRIIIa-158 SNP Sequencing

Genomic deoxyribonucleic acid (DNA) from all patients was isolated from respiratory swabs or plasma using NucliSens EasyMag extractor (BioMérieux). Genomic DNA was eluted in 50 µl nuclease-free water, followed by the FcγRIIIa-158 SNP genotyping by PCRs and Sanger-sequencing. The sequencing of the FcγRIIIa-158 SNP was performed based on a study by Murphy and colleagues [87]. To amplify the genomic DNA, containing the FcγRIIIa-158 SNP, a PCR and a nested PCR were conducted using the primers shown in table 2. The lyophilized primers (Eurofins genomics) were dissolved in sterile, nuclease-free water and diluted to a stock concentration of 100 pmol/µl.

Table 2: PCR primers used for the amplification and sequencing of the FcγRIIIa-158 SNP. Primer sequences were adopted from Murphy et al. 2015 [87].

Primer	Sequence
PCR forward	CCCTTCACAAAGCTCTGCACT
PCR reverse	ATTCTGGAGGCTGGTGCTACA
Sanger Seq forward	GTTCAAGGAGGAAGACCCTATTC
Sanger Seq reverse	TGCAAACCTACCCTGCAATC

For both the first PCR and the nested PCR, the HotStarTaq® Master Mix (QIAGEN) was used. The protocol for the first PCR is shown in table 3.

Table 3: Protocol for the first PCR using the HotStarTaq® Master Mix and forward and reverse primers to amplify the FcγRIIIa-158 SNP.

1. PCR	
HotStarTaq® Master Mix	25 µl
PCR primer forward (1:10 dilution of stock)	2.5 µl
PCR primer reverse (1:10 dilution of stock)	2.5 µl
Sample	10 µl
Nuclease-free H_2O	10 µl

Following, the first PCR was run at following settings in a MiniAmp thermocycler (Applied Biosystems):

Denaturation	95°C	15 minutes	
Annealing	60°C	1 minute	
Synthesis	72°C	2 minutes	
Denaturation	95°C	30 seconds	40 cycles
Annealing	60°C	1 minute	
Synthesis	72°C	2 minutes	
	72°C	5 minutes	
	8°C	∞	

The second PCR was a nested PCR that was performed to specifically amplify ~405 bases around the FcγRIIIa-158 SNP using Sanger primers. The protocol for the nested PCR is shown in table 4.

Table 4: Recipe for the nested PCR using the HotStarTaq® Master Mix and forward and reverse Sanger primer to amplify the product of the 1st PCR.

Nested PCR	
HotStarTaq® Master mix	40 µl
Sanger primer forward (1:10 dilution of stock)	2.5 µl
Sanger primer reverse (1:10 dilution of stock)	2.5 µl
Amplicon from first PCR	2 µl
Nuclease-free H_2O	3 µl

Following, the nested PCR was run at following settings:

Denaturation	95°C	15 minutes	
Annealing	55°C	1 minute	
Synthesis	72°C	2 minutes	
Denaturation	95°C	30 seconds	40 cycles
Annealing	55°C	1 minute	
Synthesis	72°C	2 minutes	
	72°C	5 minutes	
	8°C	∞	

The PCR amplicon from the nested PCR was visualized on a 3% agarose gel [4]. Therefore, 4 µl of the samples were mixed with 1 µl loading dye [5] and loaded onto the 3% agarose gel. The agarose gel was run at 100 volt for approximately 20 minutes. The PCR product was quantified using a DNA Molecular Weight Marker VIII 19-1114 base pair (bp) (Roche). The products were visualized using the Bio Rad GelDoxXR device. The product of the first PCR is about 1130 bp of length and the product of the nested PCR is about 405 bp of length (Figure 5).

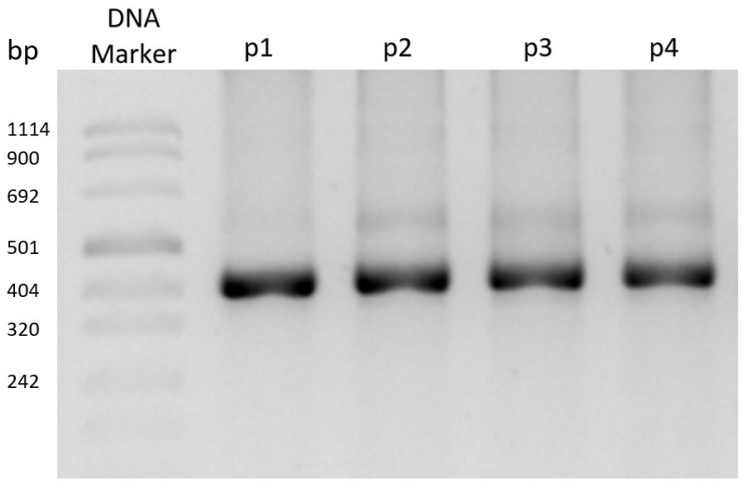

Figure 5: Representative example of four nested PCR products (product p1 – p4) with a length of ~405 base pairs and the DNA Molecular Weight Marker VIII on the left. Abbreviations: **bp**: base pair.

Following, the PCR products were prepared for Sanger sequencing. First, the amplified PCR product was cleaned enzymatically with ExoSAP-IT™ PCR Product Cleanup Reagent (Thermo Fisher Scientific). 1.5 µl of ExoSap Reagent were added to 5 µl of the PCR amplicon to remove remaining primers and nucleotides at following cycler settings:

Treatment	37°C	15 minutes
Inactivation	80°C	15 minutes
	8°C	∞

Next, the samples were diluted 1:10 with nuclease-free water for sequencing with the BigDye™ Terminator v1.1 Cycle Sequencing Kit (Thermo Fisher Scientific), according to the manufactures instruction. The BigDye Solution was prepared by mixing BigDye Terminator v1.1 and BigDye Terminator Seq Buffer v1.1 in a 1:4 ratio. 6 µl of the diluted samples were

[4] 3% agarose gel: 3 agarose tablets (0.5 g/tablet molecular biological grade 100 g; SERVA) + 50 ml 1x TBE buffer (89 mM Tris + 89 mM boric acid + 2 mM EDTA-Na_2) + 5 µl Midori Green Advance DNA stain (NIPPON Genetics)
[5] Loading dye: 100 µl glycerin + 100 µl aqua bidest + 1 crystal of bromphenol blue (Life Technologies)

mixed with 4 µl BigDye Solution and 4 µl diluted Sanger Seq primer (Table 2), either forward or reverse, with a concentration of 2 pmol/µl. The reaction ran at following settings:

Denaturation	96°C	10 seconds	25 cycles
Annealing	50°C	5 seconds	
Synthesis	60°C	4 minutes	
	8°C	∞	

Cytiva illustra™ Sephadex™ (Fisher scientific) plates were prepared to purify the PCR products from small molecules by gel filtration. 300 µl double-distilled (dd) H_2O were added to the Sephadex agarose gel and were incubated for 2 hours. The plate was centrifuged at 2600xg for 5 minutes to remove the remaining ddH_2O. The samples were added to the filters, centrifuged at 2600xg for 5 minutes and collected in a second plate filled with 25 µl of nuclease-free H_2O. The filtered and diluted DNA samples were then sequenced by the 3130 genetic analyser (Applied Biosystems) and analysed by SeqScape v2.7 (Applied Biosystems, 2009). One representative example for each FcγRIIIa-158 variant F/F, F/V and V/V is illustrated in figure 6. The quality control is used to check whether the *FCGR3B* gene is co-amplified, which could happen due to high similarity. In the *FCGR3A*, the base at the marked position is cytosine (C) and in *FCGR3B*, it is thymine (T) [87].

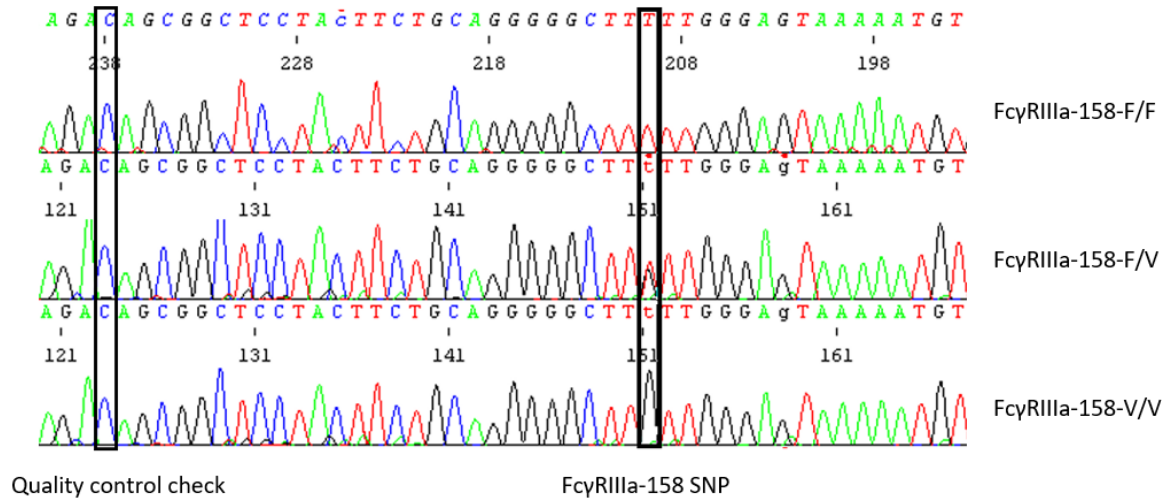

Figure 6: Representative example of an electropherogram of the three FcγRIIIa-158 variants FcγRIIIa-158-F/F (base T), FcγRIIIa-158-F/V (bases T and G) and FcγRIIIa-158-V/V (base G) marked by the square on the right side. As a quality control check, the C base is marked by the square on the left side as recommended before by Murphy et al., 2015 [86].

3.4 SARS-CoV-2-specific IgM, IgG1, IgG3, IgA1 and IgA2 ELISA

SARS-CoV-2-specific IgM, IgG1, IgG3, IgA1 and IgA2 antibodies were determined for each plasma sample by an indirect in-house ELISA. In brief, flat-bottom 96-well MaxiSorp plates (Nunc) were coated with N, S1 or S2 SARS-CoV-2 antigens (The Native Antigen) diluted to 0.5 µg/ml in carbonate coating buffer [6] overnight at 4°C. On the next day, plates were washed three times with ELISA washing buffer [7]. Following, 100 µl of diluted patients' plasma samples (1:100 dilution with PBS) were added and plates were incubated for 1 hour at 37°C. Plates were again washed three times with ELISA washing buffer and were tapped to remove all liquid. For detection, 50 µl of secondary antibodies IgM (1:4000; Goat Anti-Human IgM-HRP, Southern Biotech), IgG1 (1:1000; Mouse Anti-Human IgG1- HRP Invitrogen), IgG3 (1:1000; Mouse Anti-Human IgG3-HRP, Hinge Secondary Antibody, Invitrogen), IgA1 (1:1000; Mouse Anti-Human IgA1-HRP, Southern Biotech) or IgA2 (1:4000; Mouse Anti-Human IgA2-HRP, Southern Biotech) diluted in 5% milk powder were added and incubated for 1 hour at 37°C. Plates were again washed with ELISA washing buffer and remaining liquid was removed by tapping. 100 µl of the o-Phenylenediamine dihydrochloride (OPD) substrate [8] were added to each well of the plates. Plates were incubated for 5 minutes (IgM), for 15 minutes (IgG1, IgG3) or for 20 minutes (IgA1, IgA2) in the dark at room temperature and the reaction was stopped with 50 µl 2N H_2SO_4 [9]. Plates were analysed at an optical density (OD) of 492 nm with the Synergy HTX multi-mode reader (BioTek).

The cut-off for the determination of detectable positive antibody titers was calculated based on a study by Lunn et al. [116] with a confidence interval of 95 % in sensitivity and specificity [117]. Therefore, two standard deviations of the OD of the negative control were added to the OD value of the mean of five negative controls. Thus, an OD value of the COVID-19 patients' plasma samples above this calculated cut-off value was considered positive. Subsequently, we calculated the seroconversion rates to determine the longitudinal IgM, IgG1, IgG3, IgA1 and

[6] Carbonate coating buffer: 1.59 g/l Na_2CO_3 + 2.93 g/l $NaHCO_3$, pH = 9.6

[7] ELISA washing buffer: 1x PBS (0.8 g/l NaCl + 0.145 g/l Na_2HPO_4*$2H_2O$ + 0.02 g/l KCl + 0.02 g/L KH_2PO_4) + 0.05% Tween20, pH = 7.5

[8] OPD substrate: 9 mL 0.11 M $Na_2HPO4^*2H_2O$ (19.58 g/l) + 1 mL 0.5 M Citric Acid Monohydrate (105.1 g/l) + 10 µl H_2O_2 + 2 x 5 mg tablets OPD (Sigma-Aldrich)

[9] 2N H_2SO_4: 1 l ddH_2O + 56 ml H_2SO_4

IgA2 profile of hospitalized COVID-19 patients and seroconversion rate differences between non-hospitalized and hospitalized COVID-19 patients.

3.5 SARS-CoV-2-specific ADCC Assay

The aim of the ADCC assay was to investigate the SARS-CoV-2-specific and antibody-mediated NK cell activation. Therefore, $CD56^+CD16^+$ NK cells were incubated with either a mix of the three SARS-CoV-2-specific antigens N, S1 and S2 or a SARS-CoV-2 lysate (both: The Native Antigen) and COVID-19 patients‘ plasma samples. We evaluated two methods to determine the NK cell activation in the ADCC response: flow cytometry and ELISpot.

3.5.1 Flow Cytometry

To analyse the SARS-CoV-2-specific NK cell-mediated ADCC response, flow cytometry was performed with following pro-inflammatory cytokines (IFN-γ, TNF-α), cytotoxicity markers (CD107a, perforin) and the Live/Dead stain listed in table 5.

Table 5: Fluorescently labelled antibodies and stains used for flow cytometry with the respective laser, colour and company.

Laser	Colour	Stains	Company
FL1	FITC	LIVE/DEAD™ Fixable Green Dead Cell Stain	Invitrogen
FL2	PE	PE anti-human TNF-α Antibody	Biolegend
FL3	PerCP	PerCP anti-human CD107a (LAMP-1) Antibody	Biolegend
FL4	PE-Cy7	PE-Cy™7 Mouse Anti-Human IFN-γ	BD Pharmingen™
FL5	APC	APC Mouse Anti-Human CD56	BD Pharmingen™
FL6	APC-H7	APC-H7 Mouse Anti-Human CD16	BD Pharmingen™
FL7	BV510	Brilliant Violet 510™ anti-human Perforin Antibody	Biolegend

Isolated primary $CD56^+CD16^+$ NK cells were removed from -80°C and thawed in a 37°C water bath for 3 minutes. Cells were centrifuged at 300xg for 5 minutes in 4 ml complete RPMI medium (Sigma Aldrich) and, following, rested overnight in complete RPMI medium with 10 ng/ml IL-12 (PeproTech Austria) and 100 ng/ml IL-18 (Biozym Scientific) at a concentration of $5x10^5$ cells/ml. On the next day, cells were harvested by centrifugation at 400xg for 5 minutes, washed once with 4 ml Opti-MEM I Reduced Serum Medium (Gibco, Fisher Scientific) and resuspended in 1 ml Opti-MEM. Live cells were counted with trypan blue staining in a hemocytometer with Neubauer grid (NanoEntek) and diluted to a concentration of $5x10^5$ cells per well in a 24-well plate (Thermo Fisher Scientific) in 960 µl Opti-MEM. 30 µl of plasma (3%)

and 10 µl of diluted SARS-CoV-2 purified viral lysate (3 µg/ml) were added to a total volume of 1 ml. Next, 5 µl of the cytotoxicity marker PerCP anti-human CD107a was added and the suspension was incubated for 6 hours at 37°C. After 1 hour, Monensin (Biozym Scientific) and Brefeldin A (Biozym Scientific) were added at a concentration of 1 µl/ml to inhibit protein transport from the ER to the Golgi apparatus. After additional incubation (5 hours, 37°C, 5% CO2), stimulated cells were transferred into 15 ml falcons and wells were washed three times with 1 ml PBS. Cells were centrifuged at 400xg for 5 minutes and the supernatant was discarded. 100 µl of PBS, 2.5 µl of APC-H7 Mouse anti-human CD16, 10 µl of APC Mouse anti-human CD56 and 1 µl of LIVE/DEAD™ Fixable Green Dead Cell Stain were added. Cells were vortexed and incubated for 20 minutes in the dark at room temperature. Next, 100 µl of Fix solution (LifeTech Austria) were added and cells were incubated for 15 minutes in the dark at room temperature. Cells were collected by centrifugation at 400xg for 5 minutes after addition of 3 ml of FACS buffer [10]. After centrifugation, the supernatant was discarded and the cell pellet was dissolved in 100 µl of Permeabilization solution (LifeTech Austria). Following, 2.5 µl of each antibody PE-Cy™7 Mouse anti-human IFN-γ, PE anti-human TNF-α and Brilliant Violet 510 anti-human Perforin were added, cells were vortexed shortly and incubated for 20 minutes in the dark at room temperature. Subsequently, cells were washed by addition of 3 ml of buffer and centrifuged at 400xg for 5 minutes. Finally, the supernatant was discarded and the cell pellet was dissolved in 100 µl of FACS buffer, cells were transferred into FACS tubes (Falcon) and stored at 4°C in the dark until fluorescent analysis. NK cell activation was analysed with the BD FACSCanto II flow cytometer (BD Biosciences) using the BD FACSDiva Software (Version 6.1.1 and Version 9.0, BD Biosciences). Finally, data were evaluated using FlowJo (Version 10.7.2, FlowJo, BD Biosciences). Gates were set and NK cell activation was defined according to figure 7. The percentage of NK cell activation of all samples were normalized to the same SARS-CoV-2 seronegative control. ADCC positive plasma samples were identified using six SARS-CoV-2 seronegative controls and a 95% CI as described by Frey et al. [118].

[10] FACS Buffer: 1x PBS + 0.1% NaN_3 + 5% FCS

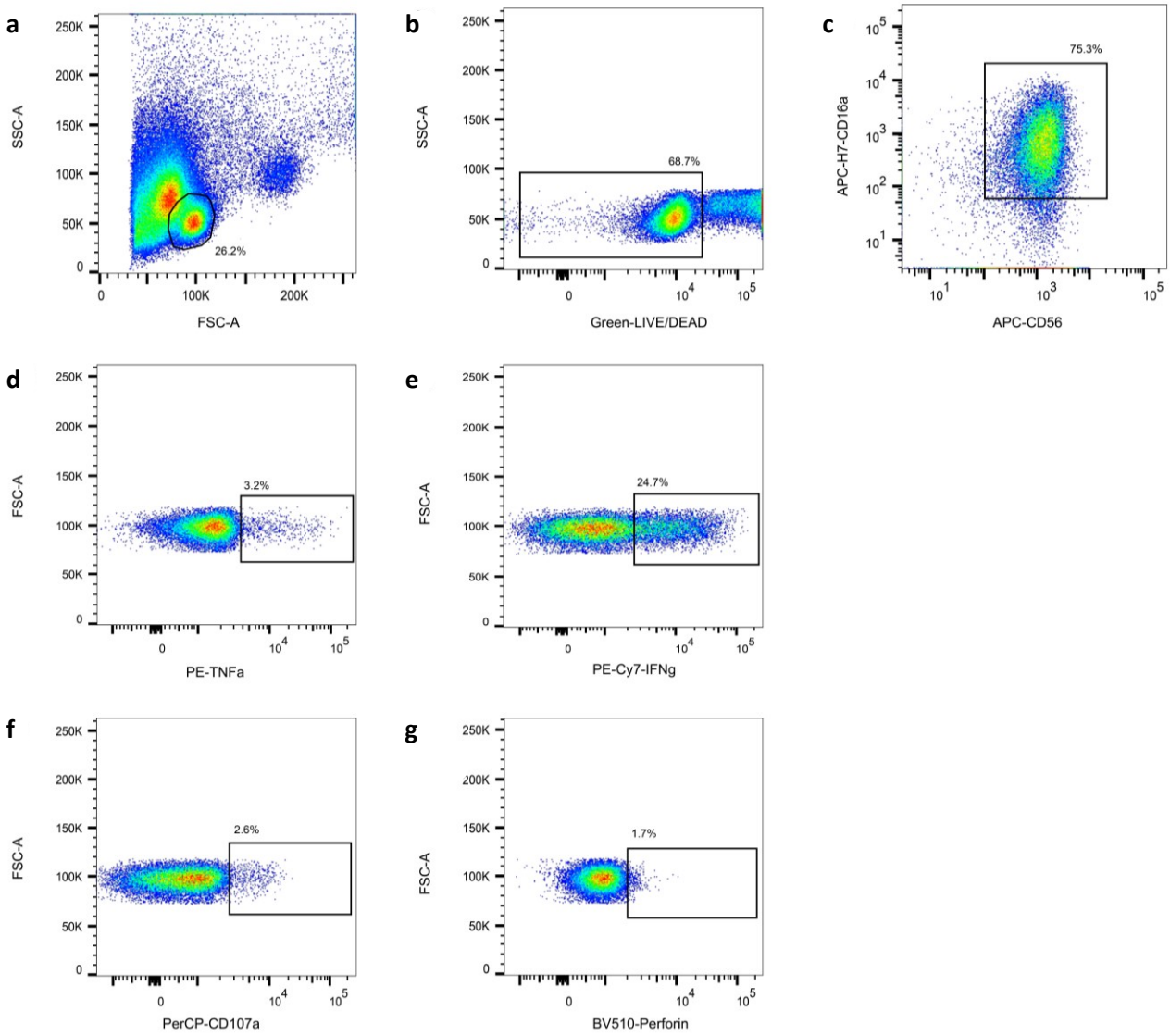

Figure 7: Gating of isolated primary CD56$^+$CD16$^+$ NK cells after flow cytometry. Gating strategy: (a) Forward and sideward scatter with the required subset representing NK cells selected. (b) Live cells were separated from dead cells with LIVE/DEAD™ Fixable Green dead cell stain (Invitrogen). (c) The CD56$^+$CD16$^+$ subset was marked by APC-CD56 and APC-H7-CD16a stain. (d) PE-TNFa, (e) PE-Cy7-IFNg, (f) PerCP-CD107a and (g) BV510-Perforin CD56$^+$CD16$^+$ NK cells.

3.5.2 IFN-γ and Perforin ELISpot

For the SARS-CoV-2-specific ADCC ELISpot assay, 96-well plates (MultiScreenHTS-IP, 0.45 µm; Merck Millipore) were treated with 200 µl 70% ethanol [11] per well for 28 minutes at room temperature. Following, plates were coated with either IFN-γ mAb 1-D1K (1 µg/ml; Mabtech) or perforin mAbs Pf-80 and Pf-164 (1 µg/ml; Mabtech) diluted with 1x PBS overnight at 4°C. During incubation, plates were wrapped in aluminium foil. On the next day, the coating solution was discarded, plates were washed three times with 300 µl of PBS per well and

[11] 70% Ethanol: ddH_2O + 70% EtOH (95 – 99%), filtration through 0.2 µm filter (Whatman)

blocked with 200 µl of a pre-warmed blocking solution [12]. Plates were again wrapped in aluminium foil and incubated for 2 hours at 37°C. Meanwhile, the three ADCC components were prepared. $CD56^+CD16^+$ NK cells were thawed in a 37°C water bath for 3 minutes and rested overnight in complete RPMI medium with 10% FCS and 10 ng/ml IL-12 and 100 ng/ml IL-18 at a concentration of $5x10^5$ cells/ml. 3% of COVID-19 patients' plasma and 3 µg/ml SARS-CoV-2 purified lysate were incubated in an additional 96-well plate for 1 hour. After removing the blocking solution and washing the plates three times with 300 µl of PBS per well, $1x10^5$ $CD56^+CD16^+$ NK cells were added to each well. Following, the plasma-lysate mix was added to each well.

Additionally, a positive control, a negative control and a blank control were included. The positive control contains 10 ng/ml IL-12 (PeproTech Austria), 10 ng/ml IL-15 (PeproTech Austria) and 10 ng/ml IL-18 (Biozym Scientific) and $CD56^+CD16^+$ NK cells without antigens and antibodies. For the negative control, stored plasma without SARS-CoV-2-specific antibodies were added to the wells. Additionally, four wells contain cells only, in order to determine the plate background. Subsequently, plates were again wrapped in aluminium foil, slightly moved horizontally and incubated for 45 hours at 37°C with 5% CO_2. After the two days incubation, the cell suspension with the antigens and antibodies was discarded and plates were first washed with 300 µl ELISpot wash buffer[13] twice and then two times with 300 µl PBS. After addition of 100 µl of the biotinylated detection antibody IFN-γ 7B6-1 (1 µg/ml; Mabtech) or perforin mAB Pf-344 (1 µg/ml; Mabtech) diluted with PBS/FCS [14], plates were incubated for 2 hours at room temperature on the shaker at 150 rpm. Subsequently, plates were washed four times with 300 µl PBS per well. Next, 100 µl streptavidin-alkaline phosphatase (1 µg/ml; Mabtech) diluted with PBS/FCS was added and filtered through Millex-GV 0.22 µm (Merck Millipore). After the plates were incubated for 45 minutes on the shaker at 150 rpm, plates were washed four times with 300 µl PBS. 100 µl of the substrate BCIP/NBT solution[15] were added and plates were incubated in the dark at room temperature for 10 minutes. The reaction was stopped by washing the plates with tapped water three times and with ddH_2O

[12] Blocking solution: 1x PBS + 5% BSA (1.5 g BSA in 30 ml PBS), filtration through 0.2 µm filter (Whatman)

[13] ELISpot wash buffer: 1x PBS + 0.05% Tween20, filtration through 0.2 µm filter (Whatman)

[14] PBS/FCS: 24.9 ml 1x PBS + 125 µl FCS, filtration through 0.2 µm filter (Whatman)

[15] BCIP/NBT solution: 1 tablet BCIP/NBT (Sigma) + 10 ml ddH_2O, vortexed and filtration through 0.2 µm filter (Whatman)

three times. Plates were kept in the dark overnight and spots were analysed on the following day with the ELISpot Bioreader 5000 (BIO-SYS).

3.6 Statistical Analysis

To compare the distribution of gender and age between the three study groups (control, non-hospitalized, hospitalized), the Chi-square test and the Kruskal-Wallis test were used. The distribution of the different FcγRIIIa-158 variants between the two COVID-19 patients' groups and the control cohort were compared using the Chi-square test. Differences between the antibody response in non-hospitalized and hospitalized COVID-19 patients were determined with a t test. Significant differences in flow cytometry data between hospitalized COVID-19 patients and the control cohort were calculated with an ANOVA and Dunn's post test. Differences between non-hospitalized COVID-19 patients and the controls were determined with a t test. A p-value <0.05 was considered significant. All statistics and figures were assessed with GraphPad Prism 5 for Windows (Version 5.04, GraphPad Software 2010, San Diego California USA, www.graphpad.com). The study was approved by the local ethics committee (EK No. 1881/2020 and 2192/2020).

4. Results

4.1 Study Cohort

In this study, respiratory swaps of in total 197 COVID-19 patients with a positive SARS-CoV-2 RT-PCR result, confirmed by a recently published real-time RT-PCR [115], were included for the sequencing of the FcγRIIIa-158 SNP. As depicted in table 6, the patient cohort was divided into two groups based on disease severity, into non-hospitalized (N=46, 45.7% female, median age: 48.8) and hospitalized persons (N=151, 35.8% female, median age: 62.2). Non-hospitalized COVID-19 patients were significantly younger than hospitalized patients ($p<0.001$, t test). Of the hospitalized cohort, 34 persons deceased during hospitalization (29.4% female, median age: 78). Deceased patients were significant older than survivors ($p=0.002$, t test). Additionally, respiratory swabs of a control cohort without any COVID-19 symptoms and with a negative SARS-CoV-2 RT-PCR result (N=99, 47.5% female, median age: 63) were included.

Table 6: Characteristics of the study cohort with the two COVID-19 groups of non-hospitalized patients (N=46) and hospitalized patients (N=151), plus the control cohort (N=99). Differences were assessed with the Chi-square test (gender) and analysis of variance (ANOVA) (age). A p-value <0.05 was considered statistically significant.

	Study Cohort			**p-value**
	Controls N=99	**Non-Hospitalized N=46**	**Hospitalized N=151**	
Female Gender (%)	Female: N=47 (47.5%)	Female: N=21 (45.7%)	Female: N=54 (35.8%)	Non-Hospitalized vs Hospitalized: p=0.23
Median Age (min-max)	63.4 (23-92)	48.8 (16-88)	62.2 (16-99)	Non-Hospitalized vs Hospitalized: p<0.001
Deceased (%) Female Gender (%) Median Age (min-max)			N=34 (22.5%) N=10 (29.4%) 78 (50-99)	Non-Deceased vs Deceased (Gender): p=0.42 Non-Deceased vs Deceased (Age): p=0.002

4.2 FcγRIIIa-158-V/V variant contributes to COVID-19 severity

For the FcγRIIIa-158 variant determination, Sanger-sequencing was performed and the distribution of the three variants FcγRIIIa-158-F/F, -F/V and -V/V was compared between the hospitalized (N=151) and non-hospitalized (N=46) COVID-19 patients and the SARS-CoV-2 PCR negative control cohort (N=99).

As shown in figure 8a, in the control cohort, 15.2% showed the FcγRIIIa-158-V/V variant, 47.5% the FcγRIIIa-158-F/V variant and 37.4% the FcγRIIIa-158-F/F variant. In hospitalized patients, the high-affinity FcγRIIIa-158-V/V variant dominated and was found significantly more often than in non-hospitalized patients. Whereas 22.5% of hospitalized patients showed the high-affinity FcγRIIIa-158-V/V variant, only 6.5% of non-hospitalized patients showed this variant. In contrast, 31.1% of hospitalized patients showed the low-affinity FcγRIIIa-158-F/F variant and 63% of non-hospitalized patients carried this variant. Concerning the heterozygous FcγRIIIa-158-F/V variant, 46.4% of hospitalized patients and 30.5% of non-hospitalized patients showed this variant. The distribution of the three FcγRIIIa variants differed significantly between hospitalized and non-hospitalized ($p=0.0003$). The distribution of the FcγRIIIa-158 variants of the non-hospitalized patient group also differed significantly from the control cohort and especially the FcγRIIIa-158-F/F occurred more frequently in non-hospitalized, compared to control patients ($p=0.01$). Differences between the hospitalized patient group and the control cohort were, however, not significant.

To analyse the role of the FcγRIIIa-158 polymorphism in COVID-19 disease severity, we also compared the distribution of the variants between the hospitalized survivors (N=117) and hospitalized deceased (N=34) COVID-19 patients (Figure 8b). Whereas of the surviving hospitalized COVID-19 patients 14.5% showed the FcγRIIIa-158-V/V variant, 50% of deceased hospitalized patients showed this high-affinity variant. In contrast, 38.5% of survivors and 5.9% of deceased showed the FcγRIIIa-158-F/F variant. The distribution of the heterozygous variant was similar with 47% of survivors and 44.1% of deceased. The difference of the distribution of the three FcγRIIIa-158 variants was significant between hospitalized survivors and hospitalized deceased with $p<0.0001$.

We then also compared the distribution of the FcγRIIIa-158 variants between hospitalized non-ICU (N=112) and hospitalized ICU (N=40) patients, as illustrated in figure 8c. The FcγRIIIa-

158-V/V variant was present in 25% of the hospitalized COVID-19 patients who required treatment on ICUs and was more frequent than in hospitalized non-ICU COVID-19 patients. In hospitalized ICU patients, the FcγRIIIa-158-F/F variant was found in only 12.5%, while the heterozygous FcγRIIIa-158-F/V variant dominated with 62.5%. In hospitalized non-ICU COVID-19 patients also the heterozygous FcγRIIIa-158-F/V variant dominated with 40.5%. In these patients, the FcγRIIIa-158-F/F variant was more frequent with 37.8% compared to FcγRIIIa-158-V/V with 21.6%. The distribution of the three FcγRIIIa-158 variants of hospitalized ICU patients differed significantly to the hospitalized non-ICU group (p=0.01).

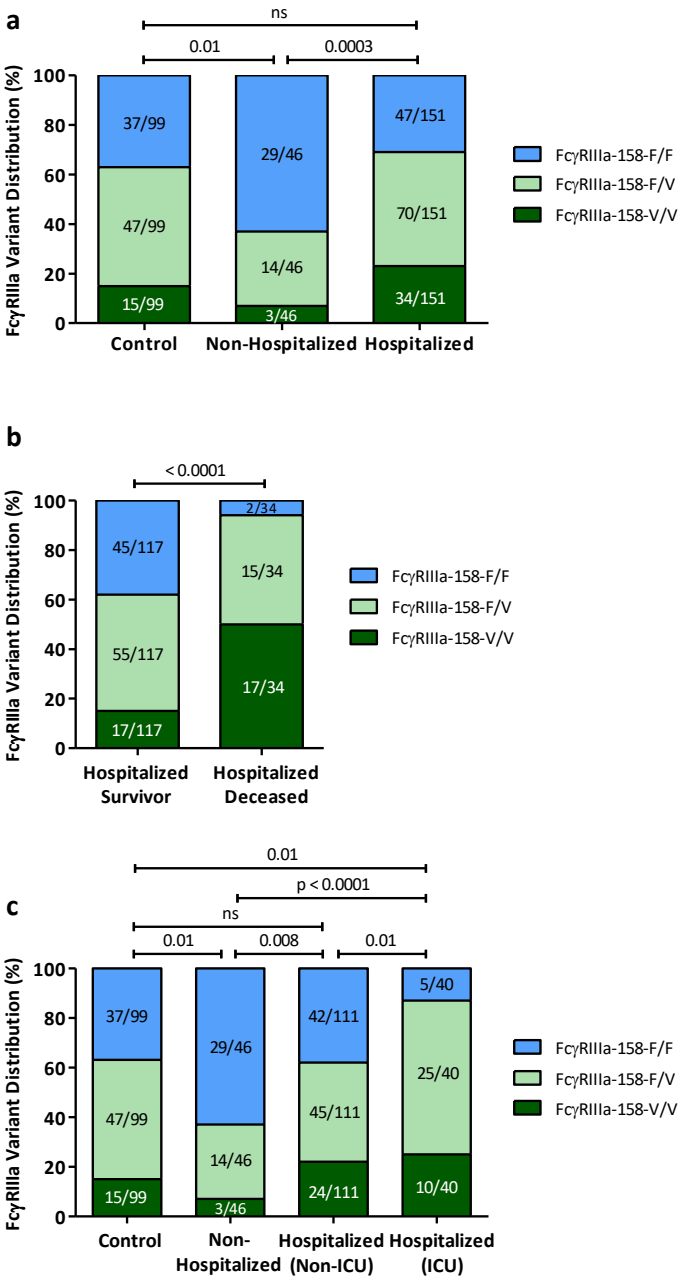

Figure 8: Distribution of the three FcγRIIIa-158 variants in the COVID-19 patient cohorts and the control group. (a) Distribution of the three FcγRIIIa-158 variants between non-hospitalized (N=46) and hospitalized (N=151) COVID-19 patients and the control group (N=99). (b) Comparison of the three FcγRIIIa-158 variants between the hospitalized survivors (N=117) and hospitalized deceased (N=34). (c) Comparison of the three FcγRIIIa-158 variants between non-hospitalized (N=46), hospitalized non-ICU (N=111) and the hospitalized ICU (N=40) COVID-19 patients and the control group (N=99). Bars represent the relative frequency (%) and in the bars are the total numbers of three variants. (a-c) The Chi-square test was used for statistical comparison between variants. The p-value <0.05 was considered significant. Abbreviations: **FcγR**: Fcγ receptor; **ICU**: intensive care unit; **ns**: not significant.

As the patients' age and gender pose critical risk factors for the development of severe COVID-19 [119], we then compared the distribution of the FcγRIIIa-158 variants between the gender and age groups.

As shown in table 7, the FcγRIIIa-158 variant distribution was significantly different between non-hospitalized and hospitalized females and males, indicating that the FcγRIIIa-158 variants are an independent risk factor for severe COVID-19 for male and female patients.

Table 7: Sex-adjusted analysis of the distribution of the FcγRIIIa-158 variants.

	Study Cohort		**P-value**[1]
	Non-Hospitalized N=46	**Hospitalized N=151**	
Female			
FcγRIIIa-158-F/F	N=14 (66.7%)	N=18 (33.3%)	**p=0.02**
FcγRIIIa-158-F/V	N=4 (19.0%)	N=27 (50.0%)	
FcγRIIIa-158-V/V	N=3 (14.3%)	N=9 (16.7%)	
Male			
FcγRIIIa-158-F/F	N=15 (60.0%)	N=29 (30.0%)	**p=0.003**
FcγRIIIa-158-F/V	N=10 (40.0%)	N=43 (44.3%)	
FcγRIIIa-158-V/V	N=0 (0.0%)	N=25 (25.7%)	

Abbreviations: **FcγR**: Fcγ receptor.

[1]Differences were assessed with the Chi-square test. The p-value <0.05 was considered significant.

We then compared the FcγRIIIa-158 variants between the age groups, as seen in table 8, and found that significant differences were mostly present between non-hospitalized and hospitalized COVID-19 patients in the younger cohort, consisting of patients <60 years of age. In the cohort of COVID-19 patients, who are older than 60 years, we could in contrast not find significant differences.

Table 8: Age-adjusted analysis of the distribution of the FcγRIIIa-158 variants.

	Study Cohort		**P-value**[1]
	Non-Hospitalized N=46	**Hospitalized N=151**	
<60 years FcγRIIIa-158-F/F FcγRIIIa-158-F/V FcγRIIIa-158-F/F	 N=19 (63.3%) N=10 (33.3%) N=1 (3.3%)	 N=13 (22.4%) N=28 (48.3%) N=17 (29.3%)	**p=0.0002**
>60 years FcγRIIIa-158-F/F FcγRIIIa-158-F/V FcγRIIIa-158-V/V	 N=10 (62.5%) N=4 (25.0%) N=2 (12.5%)	 N=34 (36.5% N=42 (45.2%) N=17 (18.3%)	p=ns

Abbreviations: **FcγR**: Fcγ receptor; **ns**: not significant.

[1]Differences were assessed with the analysis of variance (ANOVA) and Dunn's post-test. The p-value <0.05 was considered significant.

In summary, we found in our study cohort that the hospitalized COVID-19 patients showed a significantly higher frequency of the high-affinity FcγRIIIa-158-V/V variant, while non-hospitalized COVID-19 patients encoded more often for the low affinity FcγRIIIa-158-F/F. The low affinity FcγRIIIa-158-F/F variant was also dominant in hospitalized COVID-19 survivors compared to deceased, which indicates a potential protective role of the low-affinity FcγRIIIa-158-F/F variant. By analysing the FcγRIIIa-158 variant distribution in different age groups, we found significant differences mainly in the younger (<60 years) age group.

4.3 SARS-CoV-2-specific ADCC Assays

We then analysed the dynamics and extent of the SARS-CoV-2-specific antibody-dependent $CD56^{+}CD16^{+}$ NK cell response in ADCC. SARS-CoV-2-specific ADCC was measured with cytokine (IFN-γ and TNF-α) and cytotoxic (CD107a and perforin) markers by flow cytometry and by perforin secretion with an ELISpot assay.

For the *in vitro* ADCC assays by flow cytometry and ELISpot, plasma samples of in total 29 COVID-19 patients were available. This cohort was also divided into groups based on their disease severity, with 10 non-hospitalized COVID-19 patients (60% female, median: age 39.7) and 19 hospitalized COVID-19 patients (26.3% female, median age: 64). Of the 19 hospitalized

COVID-19 patients, we analysed the ADCC response over a time period of 27 days post symptoms onset (at 3 ±1 (N=7), 6 ±1 (N=14), 9 ±1 (N=15), 12 ±1 (N=18), 15 ±1 (N=18), 18 ±1 (N=18), 21 ±1 (N=15), 24 ±1 (N=11), 27 ±1 (N=7) days post symptoms onset). Of the 10 non-hospitalized COVID-19 patients, one plasma sample after 28 to 31 days post symptoms onset (median: 30 days) was available. Six SARS-CoV-2 seronegative plasma samples from the years 2014 and 2018 stored in the biobank were included as controls.

4.3.1 Flow Cytometry

The degree of SARS-CoV-2-specific $CD56^+CD16^+$ NK cell activation and the influence of the FcγRIIIa-158-F/F, -F/V and -V/V variants was investigated by flow cytometry. For the flow cytometry ADCC assays, we isolated primary $CD56^+CD16^+$ NK cells from in total 26 healthy blood donors (FcγRIIIa-158-V/V: N=5, FcγRIIIa-158-F/V: N=12, FcγRIIIa-158-F/F: N=9).

4.3.1.1 Both FcγRIIIa-158-V/V and -F/V induced higher extent of SARS-CoV-2-specific NK cell activation than FcγRIIIa-158-F/F

We first evaluated, whether the FcγRIIIa-158-F/F, FcγRIIIa-158-F/V or FcγRIIIa-158-V/V variant was associated with a higher SARS-CoV-2-specific and NK cell-mediated ADCC response. Therefore, we selected all plasma samples from hospitalized and non-hospitalized COVID-19 patients, which had a detectable ADCC response, exceeding the levels from SARS-CoV-2 seronegatives and analysed the mean fluorescence intensity (MFI) of IFN-γ, TNF-α, CD107a and perforin expressing $CD56^+CD16^+$ NK cells. Results were examined separately in the non-hospitalized COVID-19 cohort and in the hospitalized COVID-19 cohort and the MFI was normalized to one seronegative control sample.

In the hospitalized COVID-19 patients, as shown in figure 9a-d, the FcγRIIIa-158 V allele (FcγRIIIa-158-V/V and -F/V variant) was revealed to induce a higher extent of IgG-dependent NK cell activation in the longitudinal ADCC response regarding the MFI of all markers IFN-γ, TNF-α, CD107a and perforin. The results of both the FcγRIIIa-158-V/V and -F/V compared to the FcγRIIIa-158-F/F variant were significant with inclusion of all time points with positive ADCC response (all: $p<0.001$). In more detail, IFN-γ expression of $CD56^+CD16^+$ NK cells in hospitalized COVID-19 patients increased steadily and strongly after 21 days post symptoms onset and was significantly higher in both FcγRIIIa-158-F/V and -V/V compared to the FcγRIIIa-158-F/F variant, which showed steadily a low $CD56^+CD16^+$ NK cell activation (Figure 9a).

Regarding TNF-α expression, the NK cell activation with the FcγRIIIa-158-V/V and -F/V variants also differed significantly compared to FcγRIIIa-158-F/F with very low response ($p<0.001$, Figure 9b). The NK cell FcγRIIIa-158 V allele-induced activation of the cytotoxicity marker CD107a increased with time and was, including all time points, significantly higher than the NK cell activation with the FcγRIIIa-158-F/F variant with $p<0.0001$ (Figure 9c). Lastly, also perforin expression was significantly increased in hospitalized COVID-19 patients with FcγRIIIa-158 V allele variants compared to hospitalized patients with the FcγRIIIa-158-F/F variant with $p<0.001$ (Figure 9d).

Although the FcγRIIIa-158-V/V and -F/V-induced NK cell activation did not differ significantly for any markers, a slightly higher MFI was seen with the FcγRIIIa-158-V/V constantly regarding all markers. Additionally, the normalized MFI of the two FcγRIIIa-158 V allele variants was overall the highest at 24 to 27 days post symptoms onset.

As demonstrated in figure 9e-g, also in non-hospitalized patients, the V allele (FcγRIIIa-158-V/V and -F/V variants) led to a higher MFI in IFN-γ, TNF-α and CD107a expressing $CD56^+CD16^+$ NK cells after 28 to 31 days post symptoms onset. NK cells with the FcγRIIIa-158-V/V and the -F/V variants showed significantly higher production of both IFN-γ and TNF-α compared to the FcγRIIIa-158-F/F variant ($p<0.0001$) (Figure 9e+f). In CD107a expressing $CD56^+CD16^+$ NK cells, NK cells with the FcγRIIIa-158-V/V and the -F/V variant showed also a significant higher expression compared to cells with the FcγRIIIa-158-F/F variant with $p=0.006$ (Figure 9g). In contrast, the $CD56^+CD16^+$ NK cell activation measured by perforin expression was not significantly different between the three FcγRIIIa-158 variants (Figure 9h).

In addition, the normalized MFI of activated $CD56^+CD16^+$ NK cell activation elicited by non-hospitalized patients' IgG antibodies after 28 to 31 days post symptoms onset was in general lower than the one elicited by hospitalized COVID-19 patients.

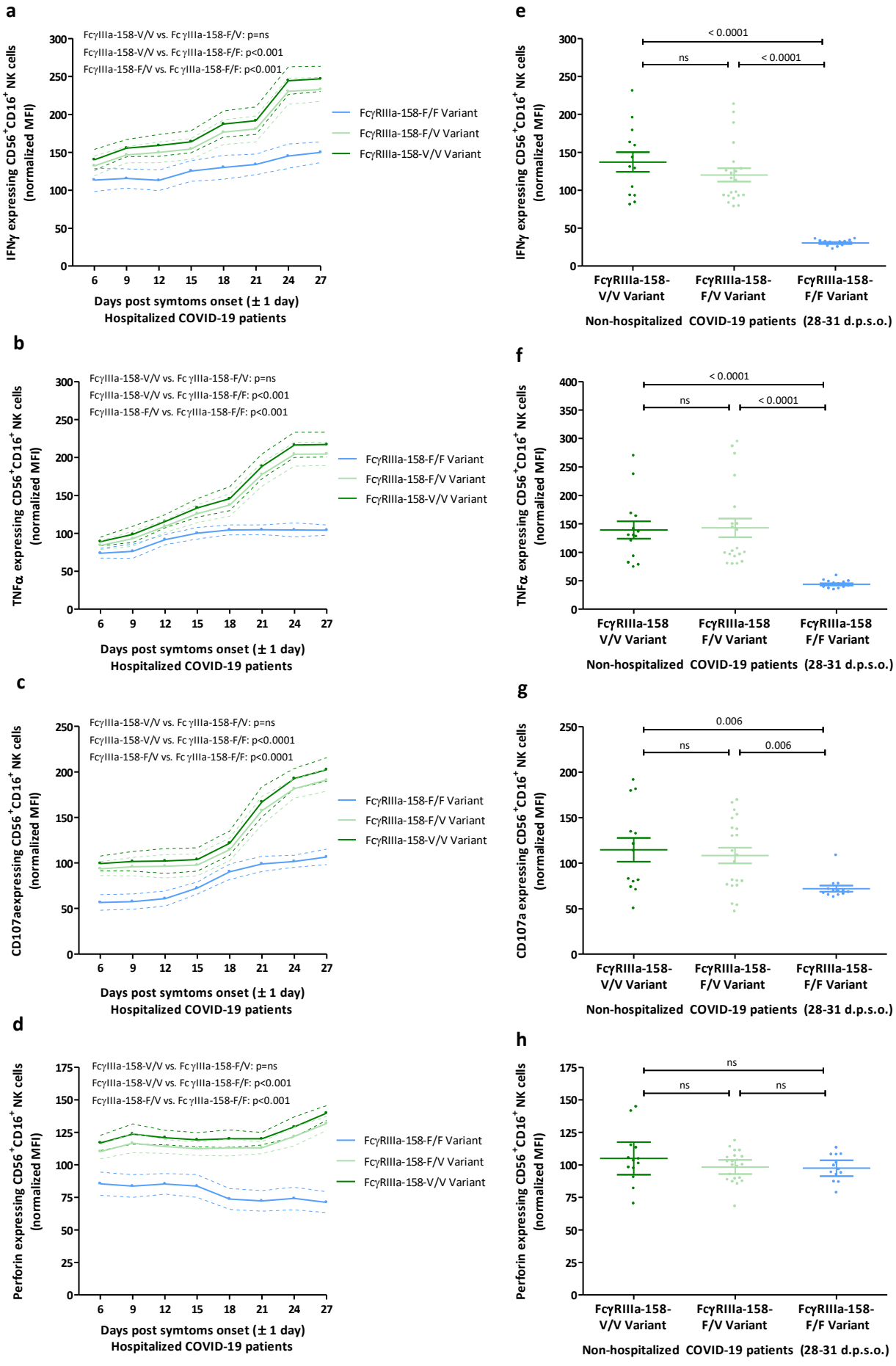

Figure 9: (continued on the following page.)

Figure 9: Analysis of the extent of the SARS-CoV-2-specific and $CD56^{+}CD16^{+}$ NK cell-mediated ADCC response with plasma obtained from (a-d) hospitalized COVID-19 patients (N=19) at 6 ±1 (N=10), 9 ±1 (N=14), 12 ±1 (N=14), 15 ±1 (N=18), 18 ±1 (N=18), 21 ±1 (N=15), 24 ±1 (N=11), 27 ±1 (N=7) days post symptoms onset or from (e-h) non-hospitalized COVID-19 patients (N=9) at 28-31 (median: 30 days) days post symptoms onset. The MFI of (a, e) IFN-γ, (b, f) TNF-α, (c, g) CD107a or (d, h) perforin positive cells was assessed by flow-cytometry. All samples were normalized to the same SARS-CoV-2 seronegative control. Data are shown as mean values (± 95% CI). (a-h) The MFI at each time point was compared between the FcγRIIIa-158-F/F, FcγRIIIa-158-F/V and FcγRIIIa-158-V/V variant by (a-d) ANOVA or (e-h) paired t test. The p-value <0.05 was considered significant. Abbreviations: **FcγR**: Fcγ receptor; **ICU**: intensive care unit; **d.p.s.o**: days post symptoms onset; **MFI**: mean fluorescence intensity; **ns**: not significant.

Taken together, FcγRIIIa-158-V/V and -F/V both lead to consistently higher IgG-mediated activation and SARS-CoV-2-specific ADCC response in both, hospitalized and non-hospitalized COVID-19 patients compared to the low affinity FcγRIIIa-158-F/F variant. Differences between the FcγRIIIa-158-V/V and -F/V variants were not significant.

4.3.1.2 ADCC responses in hospitalized COVID-19 patients are higher compared to non-hospitalized COVID-19 patients

The longitudinal profile of the overall SARS-CoV-2-specific antibody-dependent NK cell activation was analysed by flow cytometry and is demonstrated by the percentage of IFN-γ, TNF-α, CD107a and perforin expressing $CD56^{+}CD16^{+}$ NK cells, representing distinct cytotoxic and cytolytic responses. Percentages of cell activation in non-hospitalized and hospitalized COVID-19 patients were normalized to the same SARS-CoV-2 seronegative control sample and compared to six SARS-CoV-2 seronegative controls. For the SARS-CoV-2-specific antibody-dependent NK cell activation in ADCC, we considered the data of all three FcγRIIIa-158 variants.

In all hospitalized COVID-19 patients, as illustrated in figure 10a-d, a SARS-CoV-2-specific ADCC response developed within 9 days post symptoms onset, as determined by the exceeding IgG-mediated NK cell activation of SARS-CoV-2 seronegative individuals. More precisely, the SARS-CoV-2-specific ADCC response developed at 6 days post symptoms onset, as shown by IFN-γ (Figure 10a) and perforin (Figure 10d) and at 9 days post symptoms onset, as shown by TNF-α (Figure 10b) and CD107a (Figure 10c). For all ADCC markers, we observed an in general strongly increasing SARS-CoV-2-specific ADCC response, which peaked around 21 days post symptoms onset, except for CD107a. In more detail, this high increase of NK cell activation was seen after 9 days post symptoms onset for CD107a, 15 days post symptoms onset for IFN-

γ and perforin and 18 days post symptoms onset for TNF-α with a peak at day 21 post symptoms onset for the markers IFN-γ, TNF-α and perforin, followed by a plateau phase or a slight decrease. CD107a expression increased throughout the entire longitudinal analysis of 27 days post symptoms onset. Overall, SARS-CoV-2-specific IgG antibodies from hospitalized COVID-19 patients elicited the highest IFN-γ and perforin $CD56^{+}CD16^{+}$ NK cell activation.

In mildly diseased COVID-19 patients, a very low to no detectable ADCC response was found. The results of the non-hospitalized COVID-19 patient cohort can be seen in figure 10e-h. Only 44% of the mildly diseased patients showed a SARS-CoV-2-specific ADCC response elicited by IgG in the plasma 28 to 31 days post symptoms onset, exceeding the antibody-mediated NK cell activation of SARS-CoV-2 seronegative individuals. In more detail, an ADCC response of IFN-γ (Figure 10e), TNF-α (Figure 10f), CD107a (Figure 10g) and perforin (Figure 10h) expressing $CD56^{+}CD16^{+}$ NK cells was detected in 44% of non-hospitalized COVID-19 patients, respectively. Importantly, results between non-hospitalized COVID-19 patients and the SARS-CoV-2 seronegative controls were not significant.

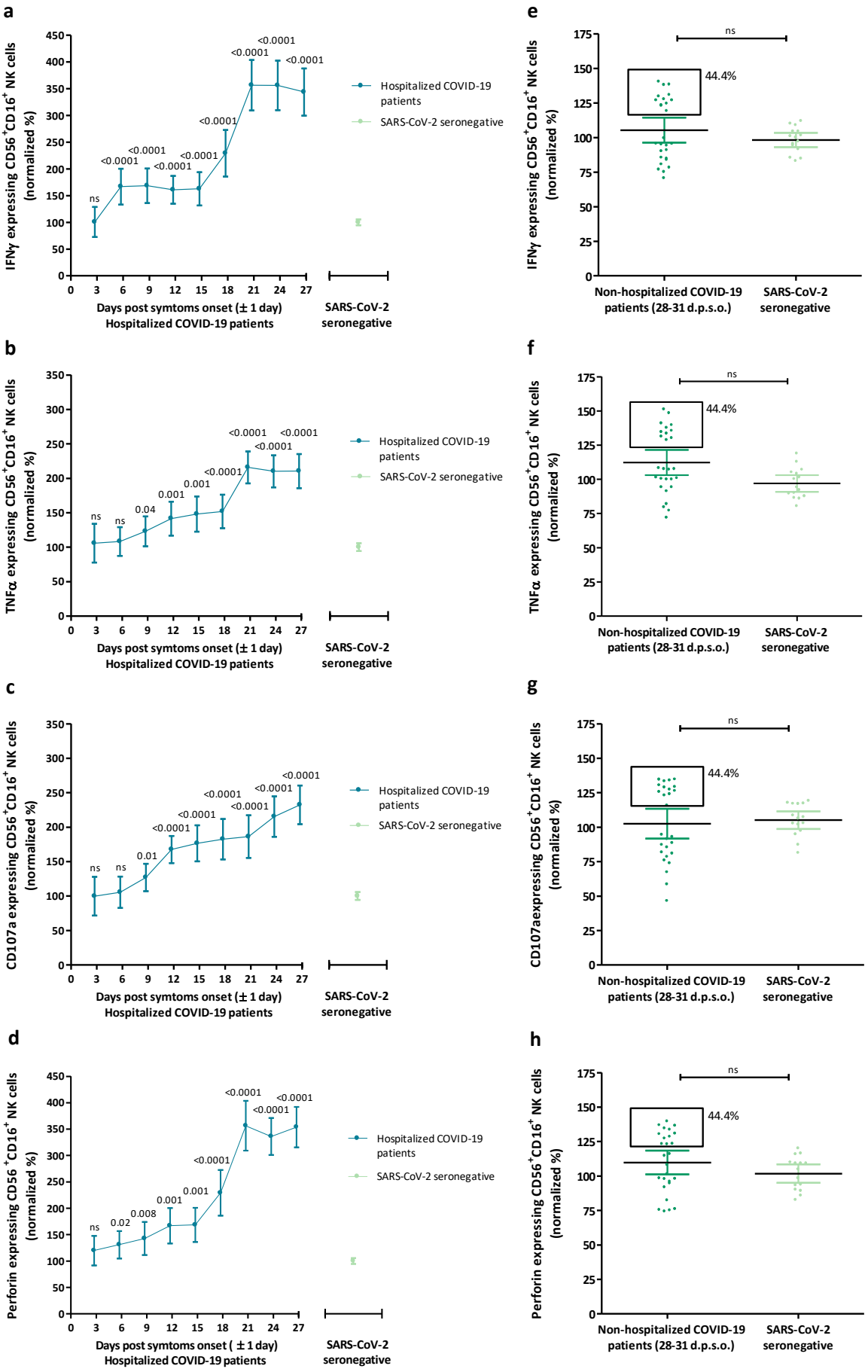

Figure 10: (continued on the following page.)

Figure 10: Analysis of the kinetics of the SARS-CoV-2-specific and $CD56^{+}CD16^{+}$ NK cell-mediated ADCC response with plasma obtained from (a-d) hospitalized COVID-19 patients (N=19) at 3 ±1 (N=7), 6 ±1 (N=14), 9 ±1 (N=15), 12 ±1 (N=18), 15 ±1 (N=18), 18 ±1 (N=18), 21 ±1 (N=15), 24 ±1 (N=11), 27 ±1 (N=7) days post symptoms onset or from (e-h) non-hospitalized COVID-19 patients (N=9) at 28-31 days (median: 30 days) days post symptoms onset. The percentages of (a, e) IFN-γ, (b, f) TNF-α, (c, g) CD107a or (d, h) perforin positive cells was assessed by flow-cytometry. All samples were normalized to the same SARS-CoV-2 seronegative control. From each sample, the median of the three FcγRIIIa-158 variants was calculated. Data are shown as mean values (± 95% CI). ADCC positive plasma samples were identified using six SARS-CoV-2 seronegative controls and a 95% CI as described by Frey et al. [118]. (a-d) The percentages of positive cells at each time point were compared between hospitalized COVID-19 patients and seronegative controls by ANOVA and Dunn's post-test. (e-h) The percentage of positive cells between non-hospitalized COVID-19 patients and seronegative controls by Mann-Whitney test. The p-value <0.05 was considered significant. Abbreviations: **d.p.s.o.**: days post symptoms onset; **ns**: not significant.

Overall, the extent of the SARS-CoV-2-specific ADCC response elicited by IgG in hospitalized COVID-19 patients' plasma was in general considerably higher than in non-hospitalized patients' plasma. Whereas hospitalized COVID-19 patients' IgG antibodies induced high activation of $CD56^{+}CD16^{+}$ NK cells with 100% of patients showing an ADCC response, only in 44% of non-hospitalized COVID-19 patients a SARS-CoV-2-specific ADCC response could be detected.

4.3.2 ADCC response detected by perforin ELISpot assay

To validate our results, we evaluated an IFN-γ- and perforin-specific ELISpot assay. Therefore, we collected plasma samples of one time point of three hospitalized COVID-19 patients. The timepoints of the three plasma samples of the hospitalized COVID-19 patients were 10, 12 and 22 days post symptoms onset, respectively. Additionally, we included one SARS-CoV-2 seronegative plasma sample as control.

The $CD56^{+}CD16^{+}$ NK cell activation in the SARS-CoV-2-specific ADCC response elicited by the plasma of three hospitalized COVID-19 patients was examined with a perforin ELISpot assay. The plasma of the three hospitalized patients elicited significantly higher $CD56^{+}CD16^{+}$ NK cell activation in ADCC compared to the SARS-CoV-2 seronegative control (Figure 11).

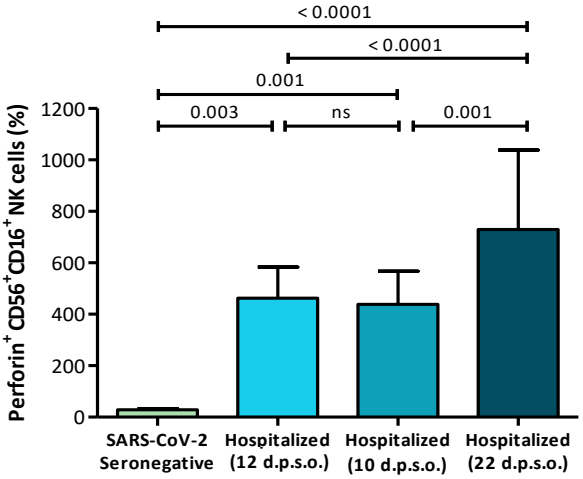

Figure 11: Comparison of the SARS-CoV-2-specific ADCC response elicited by the plasma of three hospitalized COVID-19 patients 12, 10 and 22 days post symptoms onset, respectively, and a SARS-CoV-2 seronegative control sample determined by a perforin ELISpot assay. Percentages of perforin expressing $CD56^+CD16^+$ NK cells were divided by the SARS-CoV-2 seronegative control and multiplied by 100 to get the percentages of $CD56^+CD16^+$ NK cell activation with the cut-off at 100%. The percentage of perforin expressing $CD56^+CD16^+$ NK cells was compared between the cohorts by a Fisher's exact test. The p-value <0.05 was considered significant. Abbreviations: **d.p.s.o**: days post symptoms onset; **ns**: not significant.

4.4 SARS-CoV-2-specific IgM, IgG1, IgG3, IgA1 and IgA2 antibody response

4.4.1 High SARS-CoV-2-specific IgM, IgG1 and IgG3 antibody seroconversion rates to SARS-CoV-2 N-, S1- and S2-proteins in hospitalized COVID-19 patients

We next analysed the SARS-CoV-2-specific antibody seroconversion rates in the COVID-19 patients' plasma. For the detection of SARS-CoV-2 N-, S1- and S2-antigen-specific IgM, IgG1, IgG3, IgA1 and IgA2 antibodies, in-house ELISAs were performed as decribed in the Methods' section. We selected plasma samples of in total 19 hospitalized COVID-19 patients, which were available at the biobank of the Center for Virology. Additionally, six SARS-CoV-2 seronegative plasma samples were included as controls.

In hospitalized COVID-19 patients, SARS-CoV-2-specific antibodies emerged mostly after approximately 9 to 15 days post symptoms onset, as depicted in figure 12a-c. Overall, the time of seroconversion greatly depended on the respective antibody subtype and SARS-CoV-2 antigen. IgM seroconversion occurred after 6 days post symptoms onset to the N-protein, after 12 days to S1 and after 15 days post symptoms onset to S2. 79% of hospitalized COVID-19 patients showed IgM seroconversion to SARS-CoV-2 N and S1 and 74% showed IgM seroconversion to the SARS-CoV-2 S2-protein. IgG seroconversion occurred after 12 (S1- and

S2-protein) to 15 (N-protein) days post symptoms onset. More precisely, IgG3 seroconversion could be detected after 9 days post symptoms onset to the SARS-CoV-2 N- and S2-proteins and after 12 days to the S1-protein. 74% of the hospitalized COVID-19 patients developed IgG3 antibodies specific to the SARS-CoV-2 N-protein, 58% developed SARS-CoV-2 S1-protein-specific IgG3 antibodies and 47% developed SARS-CoV-2 S2-protein-specific IgG3 antibodies. IgG1 seroconversion occurred after 12 days post symptoms onset to both the SARS-CoV-2 S1- and S2-proteins and after 15 days post symptoms onset to the SARS-CoV-2 N-protein. SARS-CoV-2-specific IgG1 seroconversion rates were in hospitalized COVID-19 patients in general lower compared to IgG3. Only 42% of the hospitalized COVID-19 patients showed IgG1 seroconversion to the SARS-CoV-2 N-protein. 37% developed IgG1 specific to the SARS-CoV-2 S1-protein and 47% developed SARS-CoV-2 S2-protein-specific IgG1 antibodies. IgA1 and IgA2 seroconversion rates were in overall low. The time point of seroconversion for IgA1 in hospitalized COVID-19 patients occurred after 6 and 12 days post symptoms onset for S1- and N-specific antibodies, respectively. In total, 32% of the hospitalized COVID-19 patients showed IgA1 antibodies to the SARS-CoV-2 N-protein and 11% to the SARS-CoV-2 S1-protein. Seroconversion for IgA2 could be detected after 9 days (N-protein) and 12 days (S1-protein) post symptoms onset. The IgA2 seroconversion rates were 26% to the SARS-CoV-2 N-protein and 21% to the SARS-CoV-2 S1-protein.

We then analysed to which SARS-CoV-2 antigen, the highest seroconversion rates in hospitalized COVID-19 patients could be detected. Whereas all hospitalized COVID-19 patients showed at least one isotype out of the five isotypes IgM, IgG1, IgG3, IgA1 and IgA2 directed to the SARS-CoV-2 N-protein, 89.7% showed antibodies directed against the SARS-CoV-2 S1-protein and 79.3% showed antibodies against the SARS-CoV-2 S2-protein. Thus, the SARS-CoV-2 N-antigen was revealed to be the main target in the overall antibody response we detected in hospitalized COVID-19 patients, followed by S1 and S2.

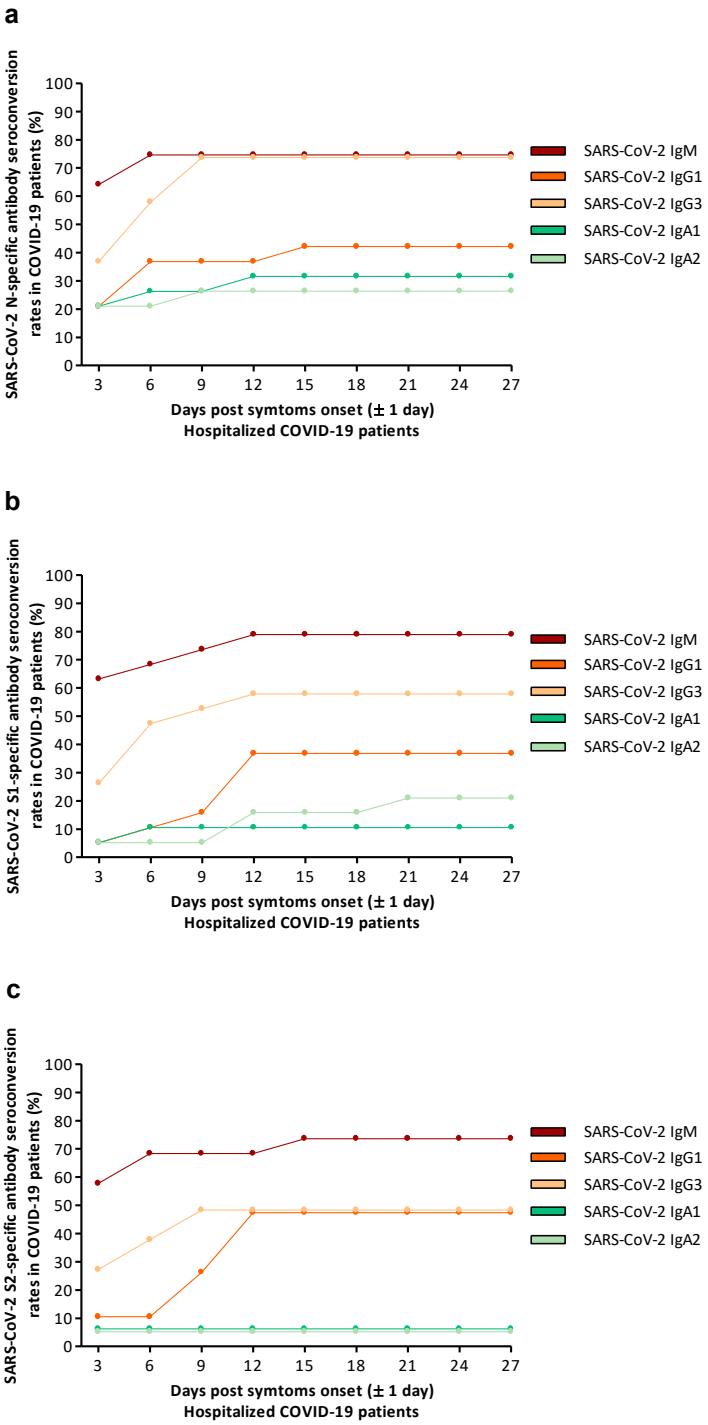

Figure 12: Analysis of the SARS-CoV-2-specific IgM, IgG1, IgG3, IgA1 and IgA2 antibody seroconversion rates directed against the SARS-CoV-2 (a) N-, (b) S1- and (c) S2-protein in the plasma obtained from (a-c) hospitalized COVID-19 patients (N=19) at 3 ±1 (N=7), 6 ±1 (N=14), 9 ±1 (N=15), 12 ±1 (N=18), 15 ±1 (N=18), 18 ±1 (N=18), 21 ±1 (N=15), 24 ±1 (N=11), 27 ±1 (N=7) days post symptoms onset assessed by ELISA. (a-c) Data are shown as percentages of COVID-19 patients who showed seroconversion after determining the cut-off by adding two standard deviations of the OD of the negative control to the OD value of the mean of five negative controls, based on a study by Lunn et al. [120] with a confidence interval of 95 % in sensitivity and specificity.

4.4.2 IgG-induced ADCC response in hospitalized COVID-19 patients

We then finally evaluated by which SARS-CoV-2-specific antibodies the NK cell-mediated ADCC response was induced. Therefore, we defined $CD56^{+}CD16^{+}$ NK cells activated in SARS-CoV-2-specific ADCC by the expression of IFN-γ. For specific analysis of the time points of positive ADCC response and IgG antibody seroconversion in hospitalized COVID-19 patients, we compared the kinetics of both IgG1 and IgG3 seroconversion rates to all three SARS-CoV-2 antigens with the IFN-γ expressing $CD56^{+}CD16^{+}$ NK cells, as illustrated in figure 13.

Whereas IgG seroconversion was detected at 9 to 15 days post symptoms onset (Figure 13a), a strong ADCC response, measured by IFN-γ^{+} $CD56^{+}CD16^{+}$ NK cells, developed later at around 21 days after onset of symptoms (Figure 13b). In more detail, IgG1 seroconversion could be detected after 6 to 15 days post symptoms onset and the IgG1 seroconversion rates were in general lower compared to IgG3. IgG3 seroconversion developed after 9 to 12 days post symptoms onset. The ADCC response, shown as IFN-γ expressing activated $CD56^{+}CD16^{+}$ NK cells was quite steady and slightly increased until day 15 post symptoms onset, followed by a strong increase until day 21 post symptoms onset and a plateau phase until day 27 post symptoms onset. Consequentially, the non-neutralizing NK cell-mediated ADCC response peaked considerably later than the SARS-CoV-2-specific IgG antibodies we detected.

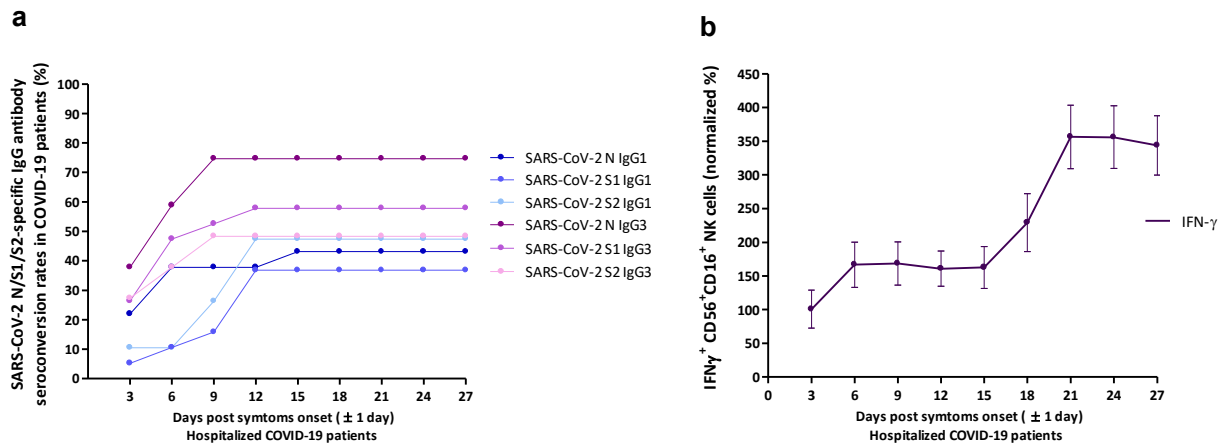

Figure 13: Demonstration of the (a) SARS-CoV-2-specific IgG1 and IgG3 antibody seroconversion rates directed against the SARS-CoV-2 N-, S1- and S2-protein and (b) the SARS-CoV-2-specific ADCC response determined by IFN-γ^{+} $CD56^{+}CD16^{+}$ NK cells in the plasma obtained from hospitalized COVID-19 patients (N=19) at 6 ±1 (N=10), 9 ±1 (N=14), 12 ±1 (N=14), 15 ±1 (N=18), 18 ±1 (N=18), 21 ±1 (N=15), 24 ±1 (N=11), 27 ±1 (N=7) days post symptoms onset.

5. Discussion

In our study, we demonstrated for the first time that a strong SARS-CoV-2-specific ADCC response may be associated with severe COVID-19 manifestations. Only limited numbers of studies about the role of NK cells in COVID-19 patients were so far available and it remained so far controversial, whether ADCC contributes to disease severity or to the clearance of SARS-CoV-2 infections [114, 117]. Using FcγRIIIa-158 SNP genotyping and *in vitro* $CD56^{+}CD16^{+}$ NK cell activation assays, we demonstrated that an overall high extent of SARS-CoV-2-specific ADCC may be linked to COVID-19 severity. Decisive for the strong SARS-CoV-2-specific ADCC response in our studies were a FcγRIIIa SNP, which leads to higher NK cell activation in SARS-CoV-2-specific ADCC, a higher antibody-mediated activation of NK cells as well as high IgG1 and IgG3 seroconversion rates directed to SARS-CoV-2 N-, S1- and S2-proteins in severely diseased COVID-19 patients.

5.1 FcγRIIIa-158-V/V was revealed as high-risk variant in COVID-19 leading to higher extent of SARS-CoV-2-specific NK cell activation

As a first major finding, we revealed that the high-affinity FcγRIIIa-158-V/V variant was significantly overrepresented in hospitalized and deceased COVID-19 patients, while the low-affinity FcγRIIIa-158-F/F variant dominated in the non-hospitalized and surviving COVID-19 patient groups. Crucially, in our study, the frequency of the three FcγRIIIa-158 variants in the control patients was comparable to that described in a recently published European study cohort [120]. While the FcγRIIIa-158-F/F and FcγRIIIa-158-F/V variants occurred frequently, the high-affinity FcγRIIIa-158-V/V variant was rare and occurred in only 15% of the controls.

By analysing the death rate in the hospitalized COVID-19 patient cohort, we found clear differences in the distribution of the FcγRIIIa-158 variants. Whereas the cohort of hospitalized survivors showed especially the low-affinity FcγRIIIa-158-F/F variant, a high number of deceased COVID-19 patients showed the high-affinity FcγRIIIa-158-V/V variant. This result underlines the potential protective role of FcγRIIIa-158-F/F and the risk of FcγRIIIa-158-V/V for COVID-19 severity as well as for COVID-19-associated death. Our results may thus indicate that the high-affinity FcγRIIIa-158-V/V variant may contribute to COVID-19 disease severity

and fatal COVID-19 outcome, while the low-affinity FcγRIIIa-158-F/F may be protective from severe SARS-CoV-2 infections and COVID-19-associated death. Importantly, using monoclonal antibodies, a recently published *in vitro* study demonstrated that the FcγRIIIa-158-V/V showed a significantly increased binding affinity to the Fc-part of IgG antibodies compared to the FcγRIIIa-158-F/F [92]. In this study, Koene et al. analysed the binding of IgG antibodies to NK cells with either the FcγRIIIa-158-F/F or the FcγRIIIa-158-V/V genotype with FITC-labelled F(ab')2 fragment of goat-antihuman-IgG and flow cytometry. Following, the study group compared the MFI of IgG1, IgG2, IgG3 and IgG4 bound by either FcγRIIIa-158-F/F NK cells or FcγRIIIa-158-V/V NK cells and significant differences could be found between these two homozygous variants for all IgG subtypes with the MFI being the highest for the IgG1-FcγRIIIa-158-V/V interaction [92]. It is thus reasonable that SARS-CoV-2-specific IgG antibodies bind with higher affinity to the FcγRIIIa-158-V/V variant, leading to a more potent NK cell activation, compared to the FcγRIIIa-158-V/F variant.

The role of the heterozygous FcγRIIIa-158-F/V in the extent of NK cell activation is, however, controversial, as shown in several studies [90–93], which demonstrated either a high-affinity or intermediate-affinity phenotype, depending on the experimental setup. In our experiment, we could not clearly define the role of the heterozygous FcγRIIIa-158-F/V variant by genetic analysis only. Although FcγRIIIa-158-F/V is more prevalent in hospitalized COVID-19 patients compared to non-hospitalized COVID-19 patients, there were no differences between the hospitalized survivors and the hospitalized non-surviving persons.

To gain insights into the extent of the $CD56^{+}CD16^{+}$ NK cell activation in SARS-CoV-2-specific ADCC induced by the three different FcγRIIIa-158 variants, we conducted an *in vitro* NK cell activation assay. Going along with the findings of Koene et al. [92], we could also show a significantly higher extent of SARS-CoV-2-specific activation of FcγRIIIa-158-V/V expressing $CD56^{+}CD16^{+}$ NK cells compared to FcγRIIIa-158-F/F expressing NK cells. Interestingly, the heterozygous FcγRIIIa-158-F/V variant induced similarly high levels of SARS-CoV-2-specific $CD56^{+}CD16^{+}$ NK cell activation as the homozygous FcγRIIIa-158-V/V did. Our *in vitro* assays thus reveal the heterozygous FcγRIIIa-158-F/V and the homozygous FcγRIIIa-158-V/V as risk factors for severe COVID-19. The importance of the presence of the V allele was also suggested by Ruyssen-Witrand et al., who showed the highest NK cell activation with FcγRIIIa-158 V allele variants and the lowest with the FcγRIIIa-158-F/F variant [93]. Further studies are, however,

needed to evaluate the impact of the heterozygous FcγRIIIa-158-F/V variant in COVID-19 disease severity.

Consequences of such a high extent of $CD56^{+}CD16^{+}$ NK cell activation are the expression of high levels of cytokines and cytotoxic proteins. Strongly activated $CD56^{+}CD16^{+}$ NK cells in SARS-CoV-2-specific ADCC with V allele variants release higher levels of IFN-γ and TNF-α, compared to FcγRIIIa-158-F/F expressing NK cells, as measured in our flow cytometry assays. The high release of pro-inflammatory cytokines may lead to extensive inflammation and COVID-19 progression. So far, multiple studies already suggested that especially TNF-α and IFN-γ are key factors in the pathogenesis of COVID-19 [56, 57, 121–124]. In COVID-19, these unusually high cytokine levels were linked to immunopathological reactions and may induce fever or myalgia in mild cases, but also life-threatening manifestations in lung, heart and kidney [123]. Elevated inflammation markers were even used prognostically to predict the requirement of mechanical ventilation, ARDS and death in hospitalized COVID-19 patients [124]. In two studies including in total 493 patients, especially TNF-α was revealed as an inflammatory cytokine, which is significantly elevated in patients with severe COVID-19 [56, 57]. Del Valle and colleagues recently identified TNF-α as a marker for cytokine storm in severe COVID-19 cases, which was also linked to fatal disease outcome [122].

It is so far unclear, which immune cells are the main source of these overshooting pro-inflammatory cytokines in the SARS-CoV-2 infected lung. We consequently speculated that TNF-α and IFN-γ are mainly produced by highly active NK cells, which is a phenomenon often seen in viral respiratory infections, such as Influenza viruses and RSV [79]. Fenggi et al. showed for example in an *in vivo* study with mice infected with RSV that increased lung injury was induced by an elevated NK cell activation and increased IFN-γ levels [79]. In COVID-19 patients, recently published studies showed overall decreased NK cells in the peripheral blood, but high NK cell levels in the BALF of severely diseased COVID-19 patients [61, 125]. It is thus reasonable that NK cells are a main source of pro-inflammatory cytokines in the SARS-CoV-2 infected lung of severely ill COVID-19 patients. It is further reasonable that especially NK cells encoding for the FcγRIIIa-158-V/V or FcγRIIIa-158-F/V variants contribute to elevated cytokine levels, hyperinflammation and an overall dysregulated innate immune response [124].

Additionally, the strong killing of SARS-CoV-2 infected cells, especially in the lung, due to high levels of proteases and cytolytic proteins released by activated NK cells in ADCC, such as

granzyme B and perforin, may excel the regenerative capacity of the lung [72]. Subsequently, lung inflammation is increased and lung injury during severe COVID-19 may occur [72]. Maucourant et al. analysed a study cohort involving 27 hospitalized COVID-19 patients [61]. They found highly active NK cells with an effector phenotype, defined by high levels of perforin and granzyme B, in COVID-19 patients with a severe course of disease. These proteases and cytolytic proteins thus eliminate infected lung epithelial cells extensively, resulting in tissue damage and severe COVID-19 manifestations [61]. In our experiments, *in vitro* flow cytometry and ELISpot assays, we also found a high SARS-CoV-2-specific expression of the cytotoxicity markers CD107a and perforin by $CD56^{+}CD16^{+}$ NK cells in ADCC elicited by hospitalized COVID-19 patients' plasma samples. In line with afore mentioned studies [60, 78], our data also suggest that there could be a critical role of exhausted effector cells, due to permanent activation, in regard of COVID-19 severity. In COVID-19 patients showing FcγRIIIa-158-V/V and FcγRIIIa-158-F/V NK cells, the cytotoxic response may be increased due to higher NK cell activation, resulting in stronger cell killing and organ injury [72].

In our study, we further identified that the FcγRIIIa-158 variants are a potential risk factor for severe COVID-19 especially in patients below the age of 60 years. This finding may be associated with the changes of the NK cell repertoire by ageing. Recently published studies showed that the elderly have an increased percentage of $CD56^{dim}CD16^{+}$ NK cells, which are highly cytotoxic. In younger individuals, $CD56^{bright}CD16^{+}$ NK cells are, however, more frequent, which possess a specialized role in cytokine production [126, 127]. These findings may indicate that elevated SARS-CoV-2-specific ADCC activity with high cytokine levels may pose a risk for disease progression especially in younger COVID-19 patients (<60 years) and that genetic variances, such as the FcγRIIIa-158 SNP, may be particularly of interest as a possible cause for poor COVID-19 outcome in these patients.

So far, different FcγRIIIa-158 variants were also seen to have an impact on disease severity in other viral diseases. In a study by Poonia et al. including 102 HIV patients, the high-affinity variant FcγRIIIa-158-V/V was associated with disease progression and constituted a greater risk for Kaposi's Sarcoma. 10% of the HIV progressors (N=59) were observed to have the high-affinity FcγRIIIa-158-V/V variant compared to 0% of the HIV suppressors (N=43) and 2.8% of the control cohort (N=70) [128].

It is important to mention that the FcγRIIIa receptor is also expressed on other immune cells, such as neutrophils, macrophages and at lesser extent on monocytes and some T cell subsets [86]. Recently published studies demonstrated the high-level activation of macrophages and especially neutrophils in the development of severe COVID-19. While in our study, we focused on the role of the NK cell-mediated SARS-CoV-2-specific ADCC responses, further studies are thus required to evaluate the SARS-CoV-2-specific ADCC response in FcγRIIIa-expressing cells, beyond the NK cell response.

5.2 Higher extent of IgG-dependent SARS-CoV-2-specific ADCC lead to severe COVID-19 manifestations

As a second major finding, we demonstrated a significantly higher extent of the overall SARS-CoV-2-specific, IgG-dependent ADCC response in hospitalized compared to non-hospitalized COVID-19 patients. In non-hospitalized COVID-19 patients, a low to even absent SARS-CoV-2-specific, IgG-dependent ADCC response was detected.

With these results, we affirm a previously published study in Chinese COVID-19 patients, which identified a higher extent of ADCC in severe compared to mild COVID-19, concluding that ADCC responses may contribute to COVID-19 pathology due to inflammation [129]. Yu et al. detected a SARS-CoV-2-specific ADCC response in COVID-19 patients, using an ADCC reporter assay, after 10 days post infection that peaked after 11-20 days and remained detectable up to 400 days post infection [129]. Further studies in asymptomatic, mild and hospitalized COVID-19 patients also found a higher SARS-CoV-2-specific ADCC activity, elicited by hospitalized COVID-19 patients' plasma compared to asymptomatic or mild COVID-19 patients' plasma. In asymptomatic COVID-19 patients an overall low SARS-CoV-2-specific ADCC response was detected [130]. Adeniji et al. recently also suggested that COVID-19 severity is associated with different SARS-CoV-2-specific IgG-mediated innate effector responses, such as ADCC [110]. The research group refers to qualitative differences of SARS-CoV-2-specific antibodies as potential contributors to COVID-19 severity. They analysed SARS-CoV-2 S1- and RBD-specific IgG-mediated ADCC in both hospitalized and non-hospitalized COVID-19 patients and found that specifically RBD-specific antibodies elicited a significantly higher ADCC response in hospitalized compared to non-hospitalized COVID-19 patients,

measured by the activation of NK cells. These SARS-CoV-2 RBD-specific ADCC responses were linked to higher levels of inflammation and immune activation markers [110]. Another study confirmed these results and demonstrated in an *in vivo* mouse study, specifically, a high RBD- and S2-mediated ADCC response and a lower NTD-specific ADCC response [129].

Overall, recently published studies and our results indicate in line that a high extent of SARS-CoV-2-specific IgG-mediated NK cell activation in ADCC and, thus, high levels of cytokines and cytotoxic proteins may lead to severe COVID-19 manifestations. In contrast, an overall lower extent of SARS-CoV-2-specific NK cell activation in ADCC with low levels of pro-inflammatory cytokines may be beneficial for the COVID-19 outcome.

5.3 Final Conclusions

In our study, we could highlight a potential negative impact of exuberant SARS-CoV-2-specific and IgG-dependent $CD56^{+}CD16^{+}$ NK cell activation for the development of severe COVID-19. The two independent key factors for such extensive NK cell-dependent ADCC responses in hospitalized COVID-19 patients may be the FcγRIIIa-158 SNP and SARS-CoV-2-specific, ADCC-mediating IgG antibodies. Concerning the FcγRIIIa-158 SNP, the FcγRIIIa-158-V/V variant may pose a genetic risk factor and the V allele was revealed to lead to higher extent of SARS-CoV-2-specific ADCC *in vitro* and, possibly, to severe COVID-19 manifestations. Consequences of elevated SARS-CoV-2-specific $CD56^{+}CD16^{+}$ NK cell activation in ADCC may be exuberant levels of inflammatory cytokines, such as IFN-γ and TNF-α, and cytotoxic proteins, such as perforin and granzyme B, which may result in hyperinflammation, extensive cell killing and organ damage, resulting in severe COVID-19 manifestations. Further studies are however required to evaluate the fine specificity of the SARS-CoV-2-specific and NK cell-mediated ADCC response to gain deeper insights into the COVID-19 immune pathogenesis.

6. References

[1] L. Q. *et al.*, “Early transmission dynamics in Wuhan, China, of novel coronavirus-infected pneumonia,” *New England Journal of Medicine*. 2020.

[2] A. G. Harrison, T. Lin, and P. Wang, “Mechanisms of SARS-CoV-2 Transmission and Pathogenesis,” *Trends in Immunology*. 2020, doi: 10.1016/j.it.2020.10.004.

[3] B. Hu, H. Guo, P. Zhou, and Z. L. Shi, “Characteristics of SARS-CoV-2 and COVID-19,” *Nature Reviews Microbiology*. 2021, doi: 10.1038/s41579-020-00459-7.

[4] World Health Organization, “WHO (COVID-19) Homepage,” 2021. https://covid19.who.int/ (accessed Dec. 14, 2021).

[5] R. Lu *et al.*, “Genomic characterisation and epidemiology of 2019 novel coronavirus: implications for virus origins and receptor binding,” *Lancet*, 2020, doi: 10.1016/S0140-6736(20)30251-8.

[6] P. V’kovski, A. Kratzel, S. Steiner, H. Stalder, and V. Thiel, “Coronavirus biology and replication: implications for SARS-CoV-2,” *Nature Reviews Microbiology*. 2021, doi: 10.1038/s41579-020-00468-6.

[7] O. Kooshkaki *et al.*, “Coronavirus Disease 2019: A Brief Review of the Clinical Manifestations and Pathogenesis to the Novel Management Approaches and Treatments,” *Frontiers in Oncology*. 2020, doi: 10.3389/fonc.2020.572329.

[8] Y. A. Malik, “Properties of coronavirus and SARS-CoV-2,” *Malaysian Journal of Pathology*. 2020.

[9] P. Zhou *et al.*, “Erratum: Addendum: A pneumonia outbreak associated with a new coronavirus of probable bat origin (Nature (1988) 81 11 (18-19)),” *Nature*. 2020, doi: 10.1038/s41586-020-2951-z.

[10] J. F. Drexler, V. M. Corman, and C. Drosten, “Ecology, evolution and classification of bat coronaviruses in the aftermath of SARS,” *Antiviral Research*. 2014, doi: 10.1016/j.antiviral.2013.10.013.

[11] Y. Guan *et al.*, “Isolation and characterization of viruses related to the SARS coronavirus from animals in Southern China,” *Science (80-.).*, 2003, doi: 10.1126/science.1087139.

[12] E. De Wit, N. Van Doremalen, D. Falzarano, and V. J. Munster, “SARS and MERS: Recent insights into emerging coronaviruses,” *Nature Reviews Microbiology*. 2016, doi:

10.1038/nrmicro.2016.81.

[13] A. A. Rabaan *et al.*, “SARS-CoV-2, SARS-CoV, and MERS-CoV: A comparative overview,” *Infezioni in Medicina*. 2020.

[14] F. Wu *et al.*, “A new coronavirus associated with human respiratory disease in China,” *Nature*, 2020, doi: 10.1038/s41586-020-2008-3.

[15] M. Y. Wang, R. Zhao, L. J. Gao, X. F. Gao, D. P. Wang, and J. M. Cao, “SARS-CoV-2: Structure, Biology, and Structure-Based Therapeutics Development,” *Frontiers in Cellular and Infection Microbiology*. 2020, doi: 10.3389/fcimb.2020.587269.

[16] S. Amor, L. Fernández Blanco, and D. Baker, “Innate immunity during SARS-CoV-2: evasion strategies and activation trigger hypoxia and vascular damage,” *Clin. Exp. Immunol.*, 2020, doi: 10.1111/cei.13523.

[17] J. Zhao, J. Qiu, S. Aryal, J. L. Hackett, and J. Wang, “The rna architecture of the sars-cov-2 3’-untranslated region,” *Viruses*, 2020, doi: 10.3390/v12121473.

[18] A. Baldassarre, A. Paolini, S. P. Bruno, C. Felli, A. E. Tozzi, and A. Masotti, “Potential use of noncoding RNAs and innovative therapeutic strategies to target the 5’UTR of SARS-CoV-2,” *Epigenomics*. 2020, doi: 10.2217/epi-2020-0162.

[19] “Biorender.” https://biorender.com/.

[20] R. Arya *et al.*, “Structural insights into SARS-CoV-2 proteins,” *Journal of Molecular Biology*. 2021, doi: 10.1016/j.jmb.2020.11.024.

[21] Q. Wang *et al.*, “Structural and Functional Basis of SARS-CoV-2 Entry by Using Human ACE2,” *Cell*, 2020, doi: 10.1016/j.cell.2020.03.045.

[22] Y. Wei, P. Aris, H. Farookhi, and X. Xia, “Predicting mammalian species at risk of being infected by SARS-CoV-2 from an ACE2 perspective,” *Sci. Rep.*, 2021, doi: 10.1038/s41598-020-80573-x.

[23] A. C. Walls, Y. J. Park, M. A. Tortorici, A. Wall, A. T. McGuire, and D. Veesler, “Structure, Function, and Antigenicity of the SARS-CoV-2 Spike Glycoprotein,” *Cell*, 2020, doi: 10.1016/j.cell.2020.02.058.

[24] L. Samavati and B. D. Uhal, “ACE2, Much More Than Just a Receptor for SARS-COV-2,” *Front. Cell. Infect. Microbiol.*, 2020, doi: 10.3389/fcimb.2020.00317.

[25] X. Zou, K. Chen, J. Zou, P. Han, J. Hao, and Z. Han, “Single-cell RNA-seq data analysis on the receptor ACE2 expression reveals the potential risk of different human organs vulnerable to

2019-nCoV infection," *Front. Med.*, 2020, doi: 10.1007/s11684-020-0754-0.

[26] G. Lebeau *et al.*, "Deciphering SARS-CoV-2 virologic and immunologic features," *International Journal of Molecular Sciences*. 2020, doi: 10.3390/ijms21165932.

[27] W. J. Wiersinga, A. Rhodes, A. C. Cheng, S. J. Peacock, and H. C. Prescott, "Pathophysiology, Transmission, Diagnosis, and Treatment of Coronavirus Disease 2019 (COVID-19): A Review," *JAMA - Journal of the American Medical Association*. 2020, doi: 10.1001/jama.2020.12839.

[28] M. Giovanetti *et al.*, "Evolution patterns of SARS-CoV-2: Snapshot on its genome variants," *Biochem. Biophys. Res. Commun.*, 2021, doi: 10.1016/j.bbrc.2020.10.102.

[29] E. Janik, M. Niemcewicz, M. Podogrocki, I. Majsterek, and M. Bijak, "The emerging concern and interest sars-cov-2 variants," *Pathogens*. 2021, doi: 10.3390/pathogens10060633.

[30] W. T. Harvey *et al.*, "SARS-CoV-2 variants, spike mutations and immune escape," *Nature Reviews Microbiology*. 2021, doi: 10.1038/s41579-021-00573-0.

[31] J. Khateeb, Y. Li, and H. Zhang, "Emerging SARS-CoV-2 variants of concern and potential intervention approaches," *Critical Care*. 2021, doi: 10.1186/s13054-021-03662-x.

[32] European Centre for Disease Prevention and Control, "COVID-19," *SARS-CoV-2 variants of concern as of 23 September 2021*. https://www.ecdc.europa.eu/en (accessed Oct. 01, 2021).

[33] A. Rambaut *et al.*, "Preliminary genomic characterisation of an emergent SARS-CoV-2 lineage in the UK defined by a novel set of spike mutations," *Virological.org*, 2020.

[34] F. Campbell *et al.*, "Increased transmissibility and global spread of SARSCoV- 2 variants of concern as at June 2021," *Eurosurveillance*, 2021, doi: 10.2807/1560-7917.ES.2021.26.24.2100509.

[35] D. A. Collier *et al.*, "Sensitivity of SARS-CoV-2 B.1.1.7 to mRNA vaccine-elicited antibodies," *Nature*, 2021, doi: 10.1038/s41586-021-03412-7.

[36] C. Ferré, V. M., Peiffer-Smadja, N., Visseaux, B., Descamps, D., Ghosn, J., & Charpentier, "Omicron variant genome evolution and phylogenetics," *J. Med. Virol.*, 2021, doi: https://doi.org/10.1002/jmv.27515.

[37] L. Guo *et al.*, "Profiling Early Humoral Response to Diagnose Novel Coronavirus Disease (COVID-19)," *Clin. Infect. Dis.*, 2020, doi: 10.1093/cid/ciaa310.

[38] M. A. Shereen, S. Khan, A. Kazmi, N. Bashir, and R. Siddique, "COVID-19 infection: Origin, transmission, and characteristics of human coronaviruses," *Journal of Advanced Research*.

2020, doi: 10.1016/j.jare.2020.03.005.

[39] H. Nishiura *et al.*, “Estimation of the asymptomatic ratio of novel coronavirus infections (COVID-19),” *International Journal of Infectious Diseases*. 2020, doi: 10.1016/j.ijid.2020.03.020.

[40] J. He, Y. Guo, R. Mao, and J. Zhang, “Proportion of asymptomatic coronavirus disease 2019: A systematic review and meta-analysis,” *J. Med. Virol.*, 2021, doi: 10.1002/jmv.26326.

[41] H. K. Lee *et al.*, “Immune transcriptomes of highly exposed SARS-CoV-2 asymptomatic seropositive versus seronegative individuals from the Ischgl community,” *Sci. Rep.*, 2021, doi: 10.1038/s41598-021-83110-6.

[42] C. Rippinger *et al.*, “Evaluation of undetected cases during the COVID-19 epidemic in Austria,” *BMC Infect. Dis.*, 2021, doi: 10.1186/s12879-020-05737-6.

[43] S. Garg *et al.*, “Hospitalization Rates and Characteristics of Patients Hospitalized with Laboratory-Confirmed Coronavirus Disease 2019 — COVID-NET, 14 States, March 1–30, 2020,” *MMWR. Morb. Mortal. Wkly. Rep.*, 2020, doi: 10.15585/mmwr.mm6915e3.

[44] S. A. Lauer *et al.*, “The incubation period of coronavirus disease 2019 (CoVID-19) from publicly reported confirmed cases: Estimation and application,” *Ann. Intern. Med.*, 2020, doi: 10.7326/M20-0504.

[45] P. Brodin, “Immune determinants of COVID-19 disease presentation and severity,” *Nature Medicine*. 2021, doi: 10.1038/s41591-020-01202-8.

[46] S. Mandal *et al.*, “Long-COVID’: A cross-sectional study of persisting symptoms, biomarker and imaging abnormalities following hospitalisation for COVID-19,” *Thorax*, 2021, doi: 10.1136/thoraxjnl-2020-215818.

[47] A. Dennis *et al.*, “Multi-organ impairment in low-risk individuals with long COVID,” *medRxiv*, 2020, doi: 10.1101/2020.10.14.20212555.

[48] Z. Gao *et al.*, “A systematic review of asymptomatic infections with COVID-19,” *Journal of Microbiology, Immunology and Infection*. 2021, doi: 10.1016/j.jmii.2020.05.001.

[49] N. S. Hendren, M. H. Drazner, B. Bozkurt, and L. T. Cooper, “Description and Proposed Management of the Acute COVID-19 Cardiovascular Syndrome,” *Circulation*, 2020, doi: 10.1161/CIRCULATIONAHA.120.047349.

[50] E. Seyed Hosseini, N. Riahi Kashani, H. Nikzad, J. Azadbakht, H. Hassani Bafrani, and H. Haddad Kashani, “The novel coronavirus Disease-2019 (COVID-19): Mechanism of action, detection

and recent therapeutic strategies," *Virology*, 2020, doi: 10.1016/j.virol.2020.08.011.

[51] Division of Population Health and National Center for Chronic Disease Prevention and Health Promotion, "COVID-19 Risks and Vaccine Information for Older Adults," 2021. https://www.cdc.gov/aging/covid19/covid19-older-adults.html (accessed Dec. 14, 2021).

[52] C. Gebhard, V. Regitz-Zagrosek, H. K. Neuhauser, R. Morgan, and S. L. Klein, "Impact of sex and gender on COVID-19 outcomes in Europe," *Biology of Sex Differences*. 2020, doi: 10.1186/s13293-020-00304-9.

[53] G. Grasselli *et al.*, "Baseline Characteristics and Outcomes of 1591 Patients Infected with SARS-CoV-2 Admitted to ICUs of the Lombardy Region, Italy," *JAMA - J. Am. Med. Assoc.*, 2020, doi: 10.1001/jama.2020.5394.

[54] E. J. Williamson *et al.*, "OpenSAFELY: factors associated with COVID-19 death in 17 million patients.," *Nature*, 2020, doi: 10.1038/s41586-020-2521-4.

[55] R. D. Molony, A. Malawista, and R. R. Montgomery, "Reduced dynamic range of antiviral innate immune responses in aging," *Experimental Gerontology*. 2018, doi: 10.1016/j.exger.2017.08.019.

[56] C. Huang *et al.*, "Clinical features of patients infected with 2019 novel coronavirus in Wuhan, China," *Lancet*, 2020, doi: 10.1016/S0140-6736(20)30183-5.

[57] C. Qin *et al.*, "Dysregulation of Immune Response in Patients with COVID-19 in Wuhan, China," *SSRN Electron. J.*, 2020, doi: 10.2139/ssrn.3541136.

[58] I. Astuti and Ysrafil, "Severe Acute Respiratory Syndrome Coronavirus 2 (SARS-CoV-2): An overview of viral structure and host response," *Diabetes Metab. Syndr. Clin. Res. Rev.*, vol. 14, no. 4, pp. 407–412, 2020.

[59] F. A. Lagunas-Rangel, "Neutrophil-to-lymphocyte ratio and lymphocyte-to-C-reactive protein ratio in patients with severe coronavirus disease 2019 (COVID-19): A meta-analysis," *Journal of Medical Virology*. 2020, doi: 10.1002/jmv.25819.

[60] N. Chen *et al.*, "Epidemiological and clinical characteristics of 99 cases of 2019 novel coronavirus pneumonia in Wuhan, China: a descriptive study," *Lancet*, 2020, doi: 10.1016/S0140-6736(20)30211-7.

[61] C. Maucourant *et al.*, "Natural killer cell immunotypes related to COVID-19 disease severity," *Sci. Immunol.*, 2020, doi: 10.1126/SCIIMMUNOL.ABD6832.

[62] C. A. Pierce *et al.*, "Immune responses to SARS-CoV-2 infection in hospitalized pediatric and

adult patients," *Sci. Transl. Med.*, 2020, doi: 10.1126/scitranslmed.abe8120.

[63] European Medicines Agency, "COVID-19 Treatments," 2021. https://www.ema.europa.eu/en/human-regulatory/overview/public-health-threats/coronavirus-disease-covid-19/treatments-vaccines/covid-19-treatments (accessed Dec. 14, 2021).

[64] European Medicines Agency, "COVID-19 Vaccines," 2021. https://www.ema.europa.eu/en/human-regulatory/overview/public-health-threats/coronavirus-disease-covid-19/treatments-vaccines/covid-19-vaccines (accessed Dec. 14, 2021).

[65] D. V. Mehrotra *et al.*, "Clinical Endpoints for Evaluating Efficacy in COVID-19 Vaccine Trials," *Ann. Intern. Med.*, 2021, doi: 10.7326/M20-6169.

[66] F. P. Polack *et al.*, "Safety and Efficacy of the BNT162b2 mRNA Covid-19 Vaccine," *N. Engl. J. Med.*, 2020, doi: 10.1056/nejmoa2034577.

[67] K. S. Corbett *et al.*, "Evaluation of the mRNA-1273 Vaccine against SARS-CoV-2 in Nonhuman Primates," *N. Engl. J. Med.*, 2020, doi: 10.1056/nejmoa2024671.

[68] S. E. Oliver *et al.*, "The Advisory Committee on Immunization Practices' Interim Recommendation for Use of Moderna COVID-19 Vaccine — United States, December 2020," *MMWR. Morb. Mortal. Wkly. Rep.*, 2021, doi: 10.15585/mmwr.mm695152e1.

[69] Moderna, "Moderna's COVID-19 Vaccine Candidate Meets its Primary Efficacy Endpoint in the First Interim Analysis of the Phase 3 COVE Study," *Press Release*, 2020.

[70] A. Kemp, "AZD1222 US Phase III trial met primary efficacy endpoint in preventing COVID-19 at interim analysis," 2021. https://www.astrazeneca.com/media-centre/press-releases/2021/astrazeneca-us-vaccine-trial-met-primary-endpoint.html.

[71] D. L. Fay, "Johnson & Johnson Announces Single-Shot Janssen COVID-19 Vaccine Candidate Met Primary Endpoints in Interim Analysis of its Phase 3 ENSEMBLE Trial Vaccine," *Angew. Chemie Int. Ed. 6(11), 951–952.*, 1967.

[72] E. Masselli *et al.*, "NK cells: A double edge sword against SARS-CoV-2," *Adv. Biol. Regul.*, 2020, doi: 10.1016/j.jbior.2020.100737.

[73] I. S. Schuster, J. D. Coudert, C. E. Andoniou, and M. A. Degli-Esposti, "'Natural Regulators': NK cells as modulators of T cell immunity," *Frontiers in Immunology*. 2016, doi: 10.3389/fimmu.2016.00235.

[74] E. Vivier, E. Tomasello, M. Baratin, T. Walzer, and S. Ugolini, “Functions of natural killer cells,” *Nature Immunology*. 2008, doi: 10.1038/ni1582.

[75] Kenneth Murphy and Casey Weaver, *Janeway’s Immunobiology*, 9th revise. New York, NY: Norton & Company, 2017.

[76] E. A. van Erp, W. Luytjes, G. Ferwerda, and P. B. van Kasteren, “Fc-Mediated Antibody Effector Functions During Respiratory Syncytial Virus Infection and Disease,” *Front. Immunol.*, vol. 10, p. urn:issn:1664–3224, 2019.

[77] S. L. H. van Dommelen, N. Sumaria, R. D. Schreiber, A. A. Scalzo, M. J. Smyth, and M. A. Degli-Esposti, “Perforin and Granzymes Have Distinct Roles in Defensive Immunity and Immunopathology,” *Immunity*, 2006, doi: 10.1016/j.immuni.2006.09.010.

[78] I. Voskoboinik, J. C. Whisstock, and J. A. Trapani, “Perforin and granzymes: Function, dysfunction and human pathology,” *Nature Reviews Immunology*. 2015, doi: 10.1038/nri3839.

[79] F. Li, H. Zhu, R. Sun, H. Wei, and Z. Tian, “Natural Killer Cells Are Involved in Acute Lung Immune Injury Caused by Respiratory Syncytial Virus Infection,” *J. Virol.*, 2012, doi: 10.1128/jvi.06209-11.

[80] G. Zhou, S. W. W. Juang, and K. P. Kane, “NK cells exacerbate the pathology of influenza virus infection in mice,” *Eur. J. Immunol.*, 2013, doi: 10.1002/eji.201242620.

[81] R. He *et al.*, “The clinical course and its correlated immune status in COVID-19 pneumonia,” *J. Clin. Virol.*, vol. 127, p. 104361, Jun. 2020, doi: 10.1016/j.jcv.2020.104361.

[82] M. Zheng *et al.*, “Functional exhaustion of antiviral lymphocytes in COVID-19 patients,” *Cellular and Molecular Immunology*. 2020, doi: 10.1038/s41423-020-0402-2.

[83] C. van Eeden, L. Khan, M. S. Osman, and J. W. C. Tervaert, “Natural killer cell dysfunction and its role in covid-19,” *International Journal of Molecular Sciences*. 2020, doi: 10.3390/ijms21176351.

[84] M. Liao *et al.*, “Single-cell landscape of bronchoalveolar immune cells in patients with COVID-19,” *Nat. Med.*, 2020, doi: 10.1038/s41591-020-0901-9.

[85] R. Moroi *et al.*, “FCGR3A-158 polymorphism influences the biological response to infliximab in Crohn’s disease through affecting the ADCC activity,” *Immunogenetics*, 2013, doi: 10.1007/s00251-013-0679-8.

[86] W. Li, H. Yang, and D. S. Dimitrov, “Identification of high-affinity anti-CD16A allotype-independent human antibody domains,” *Exp. Mol. Pathol.*, 2016, doi:

10.1016/j.yexmp.2016.10.001.

[87] K. E. Murphy, H. A. Niederer, K. S. King, E. C. Harris, S. M. Glass, and C. J. Cox, “Accurate interrogation of FCGR3A rs396991 in European and Asian populations using a widely available TaqMan genotyping method,” *Pharmacogenet. Genomics*, 2015, doi: 10.1097/FPC.0000000000000175.

[88] D. Pinto *et al.*, “Cross-neutralization of SARS-CoV-2 by a human monoclonal SARS-CoV antibody,” *Nature*, 2020, doi: 10.1038/s41586-020-2349-y.

[89] L. Quartuccio *et al.*, “The 158VV Fcgamma receptor 3A genotype is associated with response to rituximab in rheumatoid arthritis: Results of an italian multicentre study,” *Ann. Rheum. Dis.*, 2014, doi: 10.1136/annrheumdis-2012-202435.

[90] W. K. Weng and R. Levy, “Two immunoglobulin G fragment C receptor polymorphisms independently predict response to rituximab in patients with follicular lymphoma,” *J. Clin. Oncol.*, 2003, doi: 10.1200/JCO.2003.05.013.

[91] S. P. Talathi, N. N. Shaikh, S. S. Pandey, V. A. Saxena, M. S. Mamulwar, and M. R. Thakar, “FcγRIIIa receptor polymorphism influences NK cell mediated ADCC activity against HIV,” doi: 10.1186/s12879-019-4674-z.

[92] H. R. Koene *et al.*, “Fc γ RIIIa-158V/F Polymorphism Influences the Binding of IgG by Natural Killer Cell Fc γ RIIIa, Independently of the Fc γ RIIIa-48L/R/H Phenotype,” *Society*, 2014.

[93] A. Ruyssen-Witrand *et al.*, “Fcγ receptor type IIIA polymorphism influences treatment outcomes in patients with rheumatoid arthritis treated with rituximab,” *Ann. Rheum. Dis.*, 2012, doi: 10.1136/annrheumdis-2011-200337.

[94] S. Hayat, G. Babu, A. Das, Z. H. Howlader, I. Mahmud, and Z. Islam, “Fc-gamma IIIa-V158F receptor polymorphism contributes to the severity of Guillain-Barré syndrome,” *Ann. Clin. Transl. Neurol.*, 2020, doi: 10.1002/acn3.51072.

[95] F. Wu *et al.*, “Neutralizing antibody responses to SARS-CoV-2 in a COVID-19 recovered patient cohort and their implications,” *medRxiv*, 2020, doi: 10.1101/2020.03.30.20047365.

[96] P. H. Herroelen, G. A. Martens, D. De Smet, K. Swaerts, and A. S. Decavele, “Humoral Immune Response to SARS-CoV-2,” *Am. J. Clin. Pathol.*, 2020, doi: 10.1093/ajcp/aqaa140.

[97] Y.-T. Hsieh, P. Aggarwal, D. Cirelli, L. Gu, T. Surowy, and N. M. Mozier, “Characterization of FcγRIIIA effector cells used in in vitro ADCC bioassay: Comparison of primary NK cells with engineered NK-92 and Jurkat T cells,” *J. Immunol. Methods*, vol. 441, pp. 56–66, 2017.

[98] S. P. Weisberg *et al.*, “Distinct antibody responses to SARS-CoV-2 in children and adults across the COVID-19 clinical spectrum,” *Nat. Immunol.*, 2021, doi: 10.1038/s41590-020-00826-9.

[99] A. K. Azkur *et al.*, “Immune response to SARS-CoV-2 and mechanisms of immunopathological changes in COVID-19,” *Allergy: European Journal of Allergy and Clinical Immunology*. 2020, doi: 10.1111/all.14364.

[100] B. Isho *et al.*, “Persistence of serum and saliva antibody responses to SARS-CoV-2 spike antigens in COVID-19 patients,” *Sci. Immunol.*, 2020, doi: 10.1126/sciimmunol.abe5511.

[101] U. Steffen *et al.*, “IgA subclasses have different effector functions associated with distinct glycosylation profiles,” doi: 10.1038/s41467-019-13992-8.

[102] G. Vidarsson, G. Dekkers, and T. Rispens, “IgG subclasses and allotypes: From structure to effector functions,” *Front. Immunol.*, 2014, doi: 10.3389/fimmu.2014.00520.

[103] S. E. Faustini *et al.*, “Detection of antibodies to the SARS-CoV-2 spike glycoprotein in both serum and saliva enhances detection of infection,” doi: 10.1101/2020.06.16.20133025.

[104] P. Zhou *et al.*, “A pneumonia outbreak associated with a new coronavirus of probable bat origin,” *Nature*, 2020, doi: 10.1038/s41586-020-2012-7.

[105] L. Ni *et al.*, “Detection of SARS-CoV-2-Specific Humoral and Cellular Immunity in COVID-19 Convalescent Individuals,” *Immunity*, 2020, doi: 10.1016/j.immuni.2020.04.023.

[106] C. Cervia *et al.*, “Systemic and mucosal antibody responses specific to SARS-CoV-2 during mild versus severe COVID-19,” *J. Allergy Clin. Immunol.*, 2021, doi: 10.1016/j.jaci.2020.10.040.

[107] N. M. A. Okba *et al.*, “Severe Acute Respiratory Syndrome Coronavirus 2-Specific Antibody Responses in Coronavirus Disease Patients,” *Emerg. Infect. Dis.*, 2020, doi: 10.3201/eid2607.200841.

[108] Q. X. Long *et al.*, “Antibody responses to SARS-CoV-2 in patients with COVID-19,” *Nat. Med.*, 2020, doi: 10.1038/s41591-020-0897-1.

[109] T. Damelang, S. J. Rogerson, S. J. Kent, and A. W. Chung, “Role of IgG3 in Infectious Diseases,” *Trends in Immunology*. 2019, doi: 10.1016/j.it.2019.01.005.

[110] O. S. Adeniji *et al.*, “Covid-19 severity is associated with differential antibody fc-mediated innate immune functions,” *MBio*, 2021, doi: 10.1128/mBio.00281-21.

[111] L. L. Lu, T. J. Suscovich, S. M. Fortune, and G. Alter, “Beyond binding: Antibody effector functions in infectious diseases,” *Nature Reviews Immunology*. 2018, doi:

10.1038/nri.2017.106.

[112] T. Zohar and G. Alter, “Dissecting antibody-mediated protection against SARS-CoV-2,” *Nature Reviews Immunology*. 2020, doi: 10.1038/s41577-020-0359-5.

[113] F. Y. Tso *et al.*, “Presence of antibody-dependent cellular cytotoxicity (ADCC) against SARS-CoV-2 in COVID-19 plasma,” *PLoS One*, 2021, doi: 10.1371/journal.pone.0247640.

[114] M. C. Ochoa *et al.*, “Antibody-dependent cell cytotoxicity: Immunotherapy strategies enhancing effector NK cells,” *Immunology and Cell Biology*. 2017, doi: 10.1038/icb.2017.6.

[115] V. M. Corman *et al.*, “Detection of 2019 novel coronavirus (2019-nCoV) by real-time RT-PCR,” *Eurosurveillance*, 2020, doi: 10.2807/1560-7917.ES.2020.25.3.2000045.

[116] J. A. Lunn *et al.*, “Twenty two cases of canine neural angiostronglyosis in eastern Australia (2002-2005) and a review of the literature,” *Parasites and Vectors*. 2012, doi: 10.1186/1756-3305-5-70.

[117] F. T. F. Pacheco *et al.*, “Specific IgG and IgA antibody reactivities in sera of children by enzyme-linked immunoassay and comparison with giardia duodenalis diagnosis in feces,” *Ann. Lab. Med.*, 2020, doi: 10.3343/alm.2020.40.5.382.

[118] A. Frey, J. Di Canzio, and D. Zurakowski, “A statistically defined endpoint titer determination method for immunoassays,” *J. Immunol. Methods*, 1998, doi: 10.1016/S0022-1759(98)00170-7.

[119] J. Yang *et al.*, “Prevalence of comorbidities and its effects in coronavirus disease 2019 patients: A systematic review and meta-analysis,” *Int. J. Infect. Dis.*, 2020, doi: 10.1016/j.ijid.2020.03.017.

[120] A. W. Morgan *et al.*, “FcγRIIIA-158V and rheumatoid arthritis: A confirmation study,” *Rheumatology*, 2003, doi: 10.1093/rheumatology/keg169.

[121] R. Karki *et al.*, “Synergism of TNF-α and IFN-γ Triggers Inflammatory Cell Death, Tissue Damage, and Mortality in SARS-CoV-2 Infection and Cytokine Shock Syndromes,” *Cell*, 2021, doi: 10.1016/j.cell.2020.11.025.

[122] D. M. Del Valle *et al.*, “An inflammatory cytokine signature predicts COVID-19 severity and survival,” *Nat. Med.*, 2020, doi: 10.1038/s41591-020-1051-9.

[123] S. Kaur *et al.*, “The looming storm: Blood and cytokines in COVID-19,” *Blood Reviews*. 2021, doi: 10.1016/j.blre.2020.100743.

[124] J. N. Gustine and D. Jones, “Immunopathology of Hyperinflammation in COVID-19,” *American Journal of Pathology*. 2021, doi: 10.1016/j.ajpath.2020.08.009.

[125] J. W. Song *et al.*, “Immunological and inflammatory profiles in mild and severe cases of COVID-19,” *Nat. Commun.*, 2020, doi: 10.1038/s41467-020-17240-2.

[126] R. Solana, C. Campos, A. Pera, and R. Tarazona, “Shaping of NK cell subsets by aging,” *Current Opinion in Immunology*. 2014, doi: 10.1016/j.coi.2014.04.002.

[127] A. Poli, T. Michel, M. Thérésine, E. Andrès, F. Hentges, and J. Zimmer, “CD56bright natural killer (NK) cells: An important NK cell subset,” *Immunology*. 2009, doi: 10.1111/j.1365-2567.2008.03027.x.

[128] B. Poonia, G. H. Kijak, and C. D. Pauza, “High affinity allele for the gene of FCGR3A is risk factor for HIV infection and progression,” *PLoS One*, 2010, doi: 10.1371/journal.pone.0015562.

[129] Y. Yu *et al.*, “Antibody-dependent cellular cytotoxicity response to SARS-CoV-2 in COVID-19 patients,” *Signal Transduct. Target. Ther.*, 2021, doi: 10.1038/s41392-021-00759-1.

[130] J. Dufloo *et al.*, “Asymptomatic and symptomatic SARS-CoV-2 infections elicit polyfunctional antibodies,” *Cell Reports Med.*, 2021, doi: 10.1016/j.xcrm.2021.100275.

[131] E. Marklund *et al.*, “Serum-IgG responses to SARS-CoV-2 after mild and severe COVID-19 infection and analysis of IgG non-responders,” *PLoS One*, 2020, doi: 10.1371/journal.pone.0241104.

[132] H. Yu *et al.*, “Distinct features of SARS-CoV-2-specific IgA response in COVID-19 patients,” *Eur. Respir. J.*, 2020, doi: 10.1183/13993003.01526-2020.

7. List of Tables and Figures

7.1 Tables

7.2 Figures

virion and, lastly, to the exocytosis of newly formed virus particles [Figure modified from Lebeau et al. [26]].

Figure 4: NK cell effector function in ADCC in SARS-CoV-2 infection: The SARS-CoV-2 infected cell presents viral antigens on its surface. IgG antibodies thus bind to the antigens with their Fab domain and interact with the FcγRIIIa of NK cells with their Fc domain [Figure modified from van Erp et al. [76]].

Figure 5: Representative example of four nested PCR products (product p1 – p4) with a length of ~405 base pairs and the DNA Molecular Weight Marker VIII on the left. Abbreviations: **bp**: base pair.

Figure 6: Representative example of an electropherogram of the three FcγRIIIa-158 variants FcγRIIIa-158-F/F (base T), FcγRIIIa-158-F/V (bases T and G) and FcγRIIIa-158-V/V (base G) marked by the square on the right side. As a quality control check, the C base is marked by the square on the left side as recommended before by Murphy et al., 2015 [86].

Figure 7: Gating of isolated primary $CD56^+CD16^+$ NK cells after flow cytometry. Gating strategy: (a) Forward and sideward scatter with the required subset representing NK cells selected. (b) Live cells were separated from dead cells with LIVE/DEAD™ Fixable Green dead cell stain (Invitrogen). (c) The $CD56^+CD16^+$ subset was marked by APC-CD56 and APC-H7-CD16a stain. (d) PE-TNFa, (e) PE-Cy7-IFNg, (f) PerCP-CD107a and (g) BV510-Perforin $CD56^+CD16^+$ NK cells.

Figure 8: Distribution of the three FcγRIIIa-158 variants in the COVID-19 patient cohorts and the control group. (a) Distribution of the three FcγRIIIa-158 variants between non-hospitalized (N=46) and hospitalized (N=151) COVID-19 patients and the control group (N=99). (b) Comparison of the three FcγRIIIa-158 variants between the hospitalized survivors (N=117) and hospitalized deceased (N=34). (c) Comparison of the three FcγRIIIa-158 variants between non-hospitalized (N=46), hospitalized non-ICU (N=111) and the hospitalized ICU (N=40) COVID-19 patients and the control group (N=99). Bars represent the relative frequency (%) and in the bars are the total numbers of three variants. (a-c) The Chi-square test was used for statistical comparison between variants. The p-value <0.05 was considered significant. Abbreviations: **FcγR**: Fcγ receptor; **ICU**: intensive care unit; **ns**: not significant.

Figure 9: Analysis of the extent of the SARS-CoV-2-specific and $CD56^+CD16^+$ NK cell-mediated ADCC response with plasma obtained from (a-d) hospitalized COVID-19 patients (N=19) at 6 ±1 (N=10), 9 ±1 (N=14), 12 ±1 (N=14), 15 ±1 (N=18), 18 ±1 (N=18), 21 ±1 (N=15), 24 ±1 (N=11), 27 ±1 (N=7) days post symptoms onset or from (e-h) non-hospitalized COVID-19 patients (N=9) at 28-31 (median: 30 days) days post symptoms onset. The MFI of (a, e) IFN-γ, (b, f) TNF-α, (c, g) CD107a or (d, h) perforin positive cells was assessed by flow-cytometry. All samples were normalized to the same SARS-CoV-2 seronegative control. Data are shown as mean values (± 95% CI). (a-h) The MFI at each time point was compared between the FcγRIIIa-158-F/F, FcγRIIIa-158-F/V and FcγRIIIa-158-V/V variant by (a-d) ANOVA or (e-h) paired t test. The p-value <0.05 was considered significant. Abbreviations: **FcγR**: Fcγ receptor; **ICU**: intensive care unit; **d.p.s.o**: days post symptoms onset; **MFI**: mean fluorescence intensity; **ns**: not significant.

Figure 10: Analysis of the kinetics of the SARS-CoV-2-specific and $CD56^+CD16^+$ NK cell-mediated ADCC response with plasma obtained from (a-d) hospitalized COVID-19 patients (N=19) at 3 ±1 (N=7), 6 ±1 (N=14), 9 ±1 (N=15), 12 ±1 (N=18), 15 ±1 (N=18), 18 ±1 (N=18), 21 ±1 (N=15), 24 ±1 (N=11), 27 ±1 (N=7) days post symptoms onset or from (e-h) non-hospitalized COVID-19 patients (N=9) at 28-31 days

(median: 30 days) days post symptoms onset. The percentages of (a, e) IFN-γ, (b, f) TNF-α, (c, g) CD107a or (d, h) perforin positive cells was assessed by flow-cytometry. All samples were normalized to the same SARS-CoV-2 seronegative control. From each sample, the median of the three FcγRIIIa-158 variants was calculated. Data are shown as mean values (± 95% CI). ADCC positive plasma samples were identified using six SARS-CoV-2 seronegative controls and a 95% CI as described by Frey et al. [118]. (a-d) The percentages of positive cells at each time point were compared between hospitalized COVID-19 patients and seronegative controls by ANOVA and Dunn's post-test. (e-h) The percentage of positive cells between non-hospitalized COVID-19 patients and seronegative controls by Mann-Whitney test. The p-value <0.05 was considered significant. Abbreviations: **d.p.s.o.**: days post symptoms onset; **ns**: not significant.

Figure 11: Comparison of the SARS-CoV-2-specific ADCC response elicited by the plasma of three hospitalized COVID-19 patients 10, 12 and 22 days post symptoms onset, respectively, and a SARS-CoV-2 seronegative control sample determined by a perforin ELISpot assay. Percentages of perforin expressing $CD56^{+}CD16^{+}$ NK cells were divided by the SARS-CoV-2 seronegative control and multiplied by 100 to get the percentages of $CD56^{+}CD16^{+}$ NK cell activation with the cut-off at 100%. The percentage of perforin expressing $CD56^{+}CD16^{+}$ NK cells was compared between the cohorts by a Fisher's exact test. The p-value <0.05 was considered significant. Abbreviations: **d.p.s.o**: days post symptoms onset; **ns**: not significant.

Figure 12: Analysis of the SARS-CoV-2-specific IgM, IgG1, IgG3, IgA1 and IgA2 antibody seroconversion rates directed against the SARS-CoV-2 (a) N-, (b) S1- and (c) S2-protein in the plasma obtained from (a-c) hospitalized COVID-19 patients (N=19) at 3 ±1 (N=7), 6 ±1 (N=14), 9 ±1 (N=15), 12 ±1 (N=18), 15 ±1 (N=18), 18 ±1 (N=18), 21 ±1 (N=15), 24 ±1 (N=11), 27 ±1 (N=7) days post symptoms onset assessed by ELISA. (a-c) Data are shown as percentages of COVID-19 patients who showed seroconversion after determining the cut-off by adding two standard deviations of the OD of the negative control to the OD value of the mean of five negative controls, based on a study by Lunn et al. [120] with a confidence interval of 95 % in sensitivity and specificity.

Figure 13: Demonstration of the (a) SARS-CoV-2-specific IgG1 and IgG3 antibody seroconversion rates directed against the SARS-CoV-2 N-, S1- and S2-protein and (b) the SARS-CoV-2-specific ADCC response determined by $IFN\text{-}\gamma^{+}$ $CD56^{+}CD16^{+}$ NK cells in the plasma obtained from hospitalized COVID-19 patients (N=19) at 6 ±1 (N=10), 9 ±1 (N=14), 12 ±1 (N=14), 15 ±1 (N=18), 18 ±1 (N=18), 21 ±1 (N=15), 24 ±1 (N=11), 27 ±1 (N=7) days post symptoms onset.